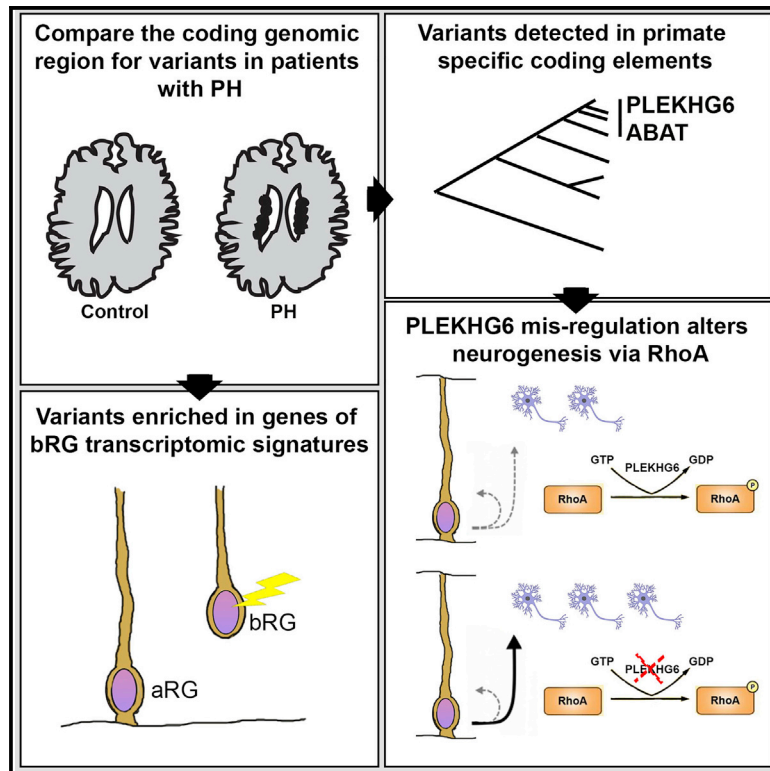


## A Primate-Specific Isoform of *PLEKHG6* Regulates Neurogenesis and Neuronal Migration

### Graphical Abstract



### Authors

Adam C. O'Neill, Christina Kyrousi, Johannes Klaus, ..., Magdalena Götz, Silvia Cappello, Stephen P. Robertson

### Correspondence

silvia\_cappello@psych.mpg.de (S.C.),  
stephen.robertson@otago.ac.nz (S.P.R.)

### In Brief

O'Neill et al. show that variants in patients with PH are enriched within genes that define basal radial glia transcriptomic signatures and provide mechanistic evidence that a primate-specific isoform of one gene, mutated in a patient with PH, regulates neurogenesis.

### Highlights

- Excess variants within basal radial glia transcriptomic signatures in cases of PH
- *PLEKHG6* primate-specific isoform mutated in a case of PH functions via RhoA
- *PLEKHG6* isoforms regulate features of neurogenesis
- Modulation of the *PLEKHG6* primate isoform reproduces features of PH in organoids



# A Primate-Specific Isoform of *PLEKHG6* Regulates Neurogenesis and Neuronal Migration

Adam C. O'Neill,<sup>1,2,3</sup> Christina Kyrousi,<sup>4</sup> Johannes Klaus,<sup>4</sup> Richard J. Leventer,<sup>5,6</sup> Edwin P. Kirk,<sup>7,8</sup> Andrew Fry,<sup>9</sup> Daniela T. Pilz,<sup>10</sup> Tim Morgan,<sup>1</sup> Zandra A. Jenkins,<sup>1</sup> Micha Drukker,<sup>2</sup> Samuel F. Berkovic,<sup>11</sup> Ingrid E. Scheffer,<sup>11,12</sup> Renzo Guerrini,<sup>13</sup> David M. Markie,<sup>14</sup> Magdalena Götz,<sup>2,3,15</sup> Silvia Cappello,<sup>4,16,17,\*</sup> and Stephen P. Robertson<sup>1,16,\*</sup>

<sup>1</sup>Department of Women's and Children's Health, University of Otago, Dunedin, New Zealand

<sup>2</sup>Institute of Stem Cell Research, Helmholtz Center, Munich, Germany

<sup>3</sup>Physiological Genomics, Biomedical Center Ludwig-Maximilians-Universitaet, Munich, Germany

<sup>4</sup>Max Planck Institute of Psychiatry, Munich, Germany

<sup>5</sup>Department of Neurology, Murdoch Children's Research Institute, Parkville, VIC, Australia

<sup>6</sup>Department of Paediatrics, University of Melbourne, Parkville, VIC, Australia

<sup>7</sup>Sydney Children's Hospital, University of New South Wales, Randwick, NSW, Australia

<sup>8</sup>New South Wales Health Pathology, Randwick, NSW, Australia

<sup>9</sup>Institute of Medical Genetics, University Hospital of Wales, Heath Park, Cardiff CF14 4XW, UK

<sup>10</sup>West of Scotland Genetics Service, Laboratory Medicine Building, Queen Elizabeth University Hospital, Glasgow G51 4TF, UK

<sup>11</sup>Epilepsy Research Centre, Department of Medicine, University of Melbourne, Austin Health, Heidelberg, VIC 3084, Australia

<sup>12</sup>The Florey Institute of Neuroscience and Mental Health, University of Melbourne, Parkville, VIC 3052, Australia

<sup>13</sup>Pediatric Neurology Unit and Laboratories, Children's Hospital A. Meyer-University of Florence, Florence, Italy

<sup>14</sup>Department of Pathology, University of Otago, Dunedin, New Zealand

<sup>15</sup>Excellence Cluster of Systems Neurology (SYNERGY), 82152 Planegg/Martinsried, Germany

<sup>16</sup>These authors contributed equally

<sup>17</sup>Lead Contact

\*Correspondence: [silvia\\_cappello@psych.mpg.de](mailto:silvia_cappello@psych.mpg.de) (S.C.), [stephen.robertson@otago.ac.nz](mailto:stephen.robertson@otago.ac.nz) (S.P.R.)

<https://doi.org/10.1016/j.celrep.2018.11.029>

## SUMMARY

The mammalian neocortex has undergone remarkable changes through evolution. A consequence of such rapid evolutionary events could be a trade-off that has rendered the brain susceptible to certain neurodevelopmental and neuropsychiatric conditions. We analyzed the exomes of 65 patients with the structural brain malformation periventricular nodular heterotopia (PH). *De novo* coding variants were observed in excess in genes defining a transcriptomic signature of basal radial glia, a cell type linked to brain evolution. In addition, we located two variants in human isoforms of two genes that have no ortholog in mice. Modulating the levels of one of these isoforms for the gene *PLEKHG6* demonstrated its role in regulating neuroprogenitor differentiation and neuronal migration via RhoA, with phenotypic recapitulation of PH in human cerebral organoids. This suggests that this *PLEKHG6* isoform is an example of a primate-specific genomic element supporting brain development.

## INTRODUCTION

Largely facilitated by changes in neural stem and progenitor cell dynamics, the mammalian neocortex has undergone remarkable modifications in size, structure, and neuronal number through evolution (Lui et al., 2011; Borrell and Reillo, 2012; Betizeau

et al., 2013; Smart et al., 2002; Lewitus et al., 2014; Borrell and Götz, 2014; Sun and Hevner, 2014; Picco et al., 2018). In the ventricular zone (VZ), apical progenitors, collectively composed of neuroepithelial cells and apical radial glia (aRG), divide to both self-renew and generate neurons (via an intermediate cell population) that migrate centrifugally to populate the cortical plate (Rakic, 1988; Malatesta et al., 2000; Noctor et al., 2001, 2004; Haubensak et al., 2004). In most primates and some non-primate species, neurogenesis also initiates with aRG; however, these cells can also divide to induce the production of another progenitor cell class called basal radial glia (bRG). Unlike their apical counterparts, bRG cells lose their VZ attachments, delaminate basally, and locate to an additional germinal layer, the outer subventricular zone (OSVZ) (Hansen et al., 2010; Fietz et al., 2010; Reillo et al., 2011). Since a strong correlation exists between regional cortical expansion and differences in abundance and properties of neuroprogenitors across species, bRG cells are proposed to constitute a major cellular substrate facilitating the evolutionary expansion of the primate cerebral cortex (Hansen et al., 2010; Fietz et al., 2010; Reillo et al., 2011). A consequence of these rapid, expansive cortical evolutionary events, particularly in humans, could be a trade-off that has rendered the brain susceptible to certain neurodevelopmental and neuropsychiatric conditions (Bae et al., 2014; Doan et al., 2016; Bershteyn et al., 2017). Data from humans with such disorders could therefore provide insight into recently evolved genetic substrates for cerebral cortical complexification.

Periventricular nodular heterotopia (PH) is a structural malformation of cortical development, characterized by a failure of some neurons to locate correctly within the cerebral cortex; instead, they adopt heterotopic positions close to their sites of



**Table 1. Observed and Expected *De Novo* Variants Identified in Patients with PH in Genes that Are Differentially Expressed in aRG and bRG**

| Gene Set | No. of Genes | PH (n = 65) |     |        |
|----------|--------------|-------------|-----|--------|
|          |              | Exp         | Obs | p      |
| aRG      | 33           | 0.14        | 1   | 0.133  |
| bRG      | 67           | 0.26        | 2   | 0.024* |

Exact binomial test (two-tailed). Exp, expected; obs, observed. Asterisk (\*) indicates significant p value.

production, the margins of the lateral ventricles (Guerrini and Dobyns, 2014). PH has traditionally been viewed as a disorder of abnormal migration, but recent data have outlined a role for disorganized neural stem cell dynamics in its causation (Cappello et al., 2013; Kielar et al., 2014). Mouse models often fail to recapitulate human forms of PH, suggesting that species-specific differences, including evolutionarily dynamic mechanisms, could underpin its pathogenesis (Feng et al., 2006; Hart et al., 2006; Corbo et al., 2002; Johnson et al., 2018).

A recent study in which the coding region of the genome (the exome) was sequenced in 202 individuals with PH, and their unaffected parents demonstrated a substantial, albeit highly heterogeneous, genetic component contributing to the etiology of the condition (Heinzen et al., 2018). Such heterogeneity makes the discovery of new loci and cellular processes underpinning its cause difficult. In this study, we sought to test the hypothesis that variants in recently evolved exomic elements contribute to the pathogenesis of PH. To investigate this, our hypotheses were 2-fold. First, we hypothesized that genes defining a differential expression signature for basal progenitors (specifically bRG), but not their apical counterparts (aRG), are enriched for genetic variants identified in individuals with PH. Second, we proposed that rare variants in individuals with PH would be found in human and/or primate exomic elements that have no mouse ortholog, representing newly evolved regions of the human and/or primate coding genome that have properties that influence neurogenesis. Although the genetic heterogeneity underlying PH would likely preclude such loci fulfilling criteria for pathogenicity (Heinzen et al., 2018), demonstration of their cellular functions could nevertheless implicate them as newly evolved contributors to cortical development.

To this end, we demonstrate here that *de novo* coding variants identified in individuals with PH are located in genes associated with bRG, but not aRG, function. Furthermore, genetic variants identified in individuals with PH do occur in isoforms with no ortholog in mice. Although falling short of proof of pathogenicity on genetic grounds, forced expression of one of these isoforms in *PLEKHG6* in the developing mouse cortex promoted defects in cellular proliferation and neuronal migration via activating RhoA, a gene whose knockout is associated with neuronal heterotopia (Cappello et al., 2012). Furthermore, modulating the specific isoform of interest in *PLEKHG6* phenotypically recapitulates PH in human cerebral organoids. These results indicate a role for bRG in PH etiology, demonstrate the utility of functional assays in further investigating the relevance of candidate disease gene loci in genetically heterogeneous conditions, and

highlight a primate-specific genomic element in the gene *PLEKHG6* in brain development.

## RESULTS

### Enhanced Burden of *De Novo* Variants in Individuals with PH in Genes Associated with Basal Radial Glia Cell Identity

To determine whether variants detected within the exomes of individuals with PH localize to recently evolved genomic sequences, we independently aligned and variant called exomes on a cohort of 65 proband-parent trios we recruited and identified 67 variants (50 *de novo*, 17 biallelic variants) not observed within control datasets (Lek et al., 2016; Sherry et al., 2001; Auton et al., 2015) (Tables S1 and S2). This cohort was a subfraction of a larger collection of individuals with PH that were separately analyzed on an independent platform as part of a study on the genetic etiology of PH (Heinzen et al., 2018).

Given that primate brain complexification is linked to basal radial glia (bRG) expansion, we questioned whether elevated rates of variants were observed in genes that exhibit expression signatures linked to bRG cell function. Transcriptional signatures that can distinguish bRG from their apical counterparts (aRG) have been defined (Pollen et al., 2015; Florio et al., 2015; Nowakowski et al., 2017). Intersecting this gene set with loci with *de novo* variants identified in our exome dataset yielded two genes as common between the two groups, a significant excess compared to the expectation on the basis of gene-specific rates of variation ( $p = 0.024$ , exact binomial test; Table 1). In contrast, when the same loci were intersected across the 33 aRG-associated genes (Pollen et al., 2015), only one, *LRIG3*, was shared in common ( $p = 0.133$ , exact binomial test; Table 1). The distribution of non-synonymous *de novo* variants per patient also closely approximated that expected by a Poisson distribution of random mutational events, and all *de novo* events were confirmed by an orthogonal technique. The rate of synonymous variants also did not significantly deviate from the 0.27 events per exome expected ( $p = 0.527$ , exact binomial test). These data indicate that the burden associations described here are not driven by variant over-calling. Previous studies of populations with various neurodevelopmental and neuropsychiatric disorders have also observed an enrichment of identified *de novo* mutations in various gene sets (Bayés et al., 2011; Darnell et al., 2011; Feldman et al., 2008; Iossifov et al., 2012, 2014; Kang et al., 2011; Voineagu et al., 2011). When compared to the genes with variants in this study, no enrichment of *de novo* events was observed (Table S3), strengthening the specificity of our finding related to bRG function.

### Exomic Variants Detected in Individuals with PH within Recently Evolved Regions of the Coding Genome

The observation that PH may result from mutations in genes that have recently acquired adaptive functions in the brain could be indicative of a more widespread phenomenon—that PH etiology could be related closely to developmental vulnerabilities conferred by recently evolved genetic elements. Although loci identified using this approach may fall short of proof of pathogenicity on genetic grounds, such a hypothesis

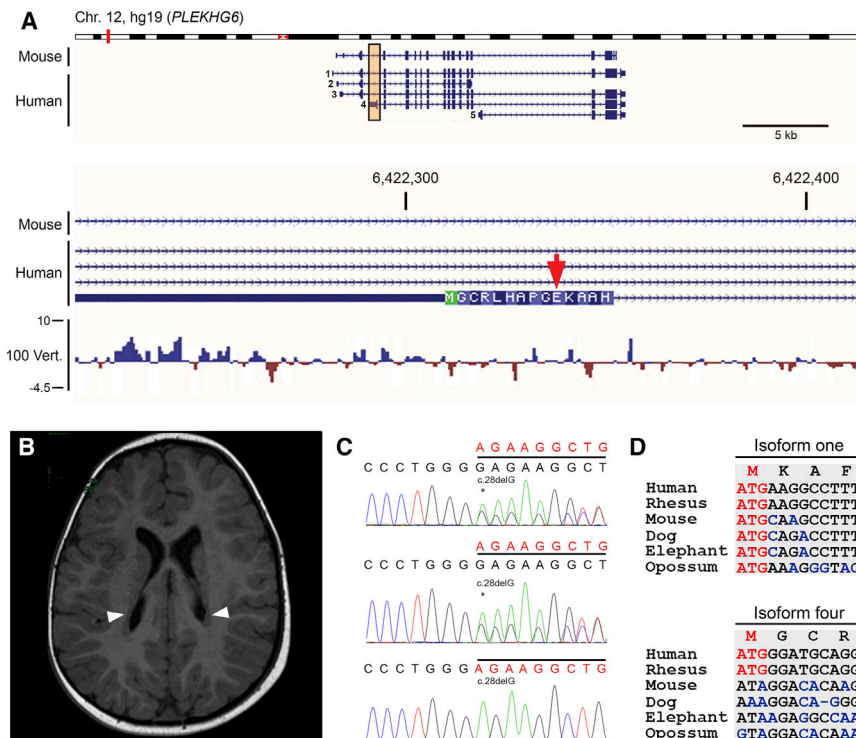


**Figure 1. Biallelic Knockout of a Primate-Specific Isoform of *PLEKHG6* in an Individual with PH**

(A) University of California, Santa Cruz (UCSC) Genome Browser tracks illustrating the *PLEKHG6* locus and the deletion identified in a patient with PH in an isoform that is present in humans, but not mice. Top: the entire locus and all of the isoforms annotated in mice and humans are outlined. Orange box highlights the region shown at higher resolution at bottom. Red arrow identifies the site of the frameshift variant in *PLEKHG6* isoform 4 for which the index case is homozygous (Table S2). 100 Vert. track depicts multiple alignment data for 100 vertebrate species and measurements of evolutionary conservation (Rosenbloom et al., 2015).

(B) Axial brain MRI scan of an individual homozygous for the c.28delG variant in *PLEKHG6* isoform 4. White arrowheads mark the presence of bilateral, posterior-predominant, periventricular nodular heterotopia.

(C) Sequence traces illustrating the sequence variant c.28delG, present in a homozygous and heterozygous state in the index case (bottom trace) and parents (top two traces), respectively.

(D) Sequence homology observed at the transcriptional start sites of isoforms 1 and 4 in the indicated species.

could inform the function of newly evolved regions of the human and/or primate coding genome and represent candidate disease loci for further investigation, especially if associated with cellular pathways already implicated in PH. To test this hypothesis, we filtered for variants that are located within validated human transcripts (the Consensus Coding Sequence [CCDS] [Pruitt et al., 2009]) that have no ortholog in mice. We identified two variants in two different genes—one in *ABAT* (*de novo* missense variant c.1426T>G [p.Ser476Ala]; RefSeq NM\_001127448) and *PLEKHG6* (homozygosity for c.28delG [p.Glu10Argfs\*40]; RefSeq NM\_001144857.1) (Figures 1A and S1A). Since the variant identified in *ABAT* is missense and therefore difficult to *a priori* assign functional significance to, we focused on the loss-of-function genotype in *PLEKHG6* (Figure 1C), a gene that encodes the guanine nucleotide exchange factor (pleckstrin homology domain containing family G member 6), as a potential novel locus regulating neurogenesis in humans. *PLEKHG6* is an activator of the small Ras homologous guanosine triphosphatase (RhoGTPase) RhoA (Asiedu et al., 2009), the conditional depletion of which within the developing mouse forebrain is associated with neuronal heterotopia (Capello et al., 2012).

The proband with the homozygous frameshift variant in *PLEKHG6* was diagnosed as having intellectual disability and bilateral PH predominantly affecting the trigone, posterior, and temporal horns of the lateral ventricles (Figure 1B; Table S4). This patient also had no pathogenic variants identified in known loci previously implicated in PH, including *FLNA*. Congruent with studies that place *PLEKHG6* beyond the 90<sup>th</sup> percentile for genes exhibiting purifying selection (Huang et al., 2010; Petrov-

ski et al., 2013), only two homozygous loss-of-function (LoF) events are observed in *PLEKHG6* in the Genome Aggregation Database (gnomAD; representing 123,136 exome and 15,496 genome sequences from unrelated individuals) (Lek et al., 2016). One of the individuals had the same genotype identified in the present study, although their phenotypic status is unknown. It is noteworthy that the individual in this study has mild cognitive disability but no seizures, and therefore it is possible that the individual listed in gnomAD may have a similar or subclinical phenotype. Such instances have been documented for other loci implicated in the causation of PH (Heinzen et al., 2018). These findings therefore represent a *prima facie* case for this biallelic genotype associated with PH to be of functional significance.

### ***PLEKHG6* Isoforms Are Differentially Expressed in Neural Progenitors and Neurons of Developing Human Brains and Organoids**

In humans, *PLEKHG6* encodes at least five alternate transcripts (Figure 1A), three of which have initiation codons within exon 2. Isoforms 4 and 5, however, use unique first exons and consequently encode proteins with novel N termini (Figures 1A and 1D). Transcriptional start sites directing the production of isoforms 4 and 5 are confined to primates (Figures 1D and S1B), indicating that this regulatory innovation arose after the divergence of primates from other mammalian species 65–85 million years ago. The biallelic frameshift variant observed in the individual with PH lies in the exon 1-specifying transcript 4 (*PLEKHG6\_4*) of human *PLEKHG6* and predicts nullizygosity for this isoform.



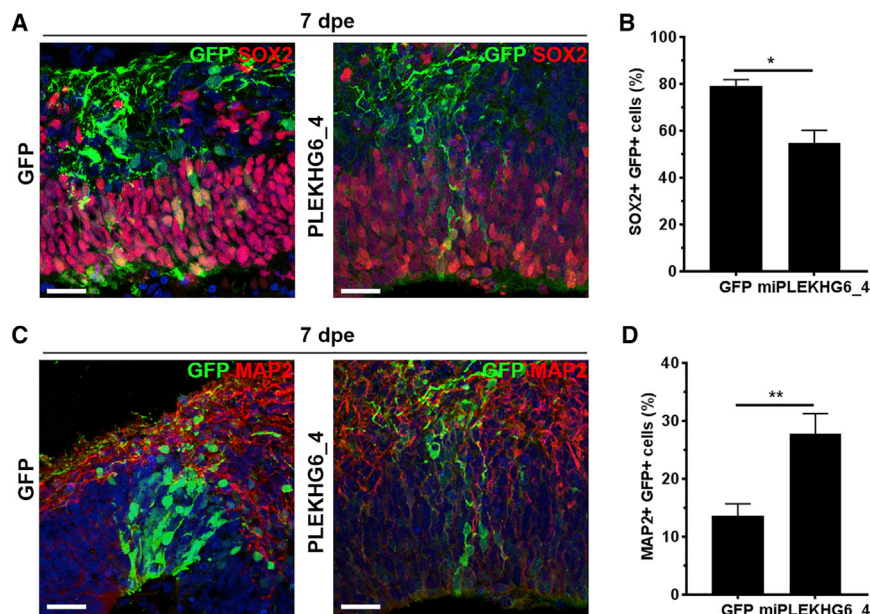


**Figure 2. PLEKHG6\_4 Knockdown in Human Cerebral Organoids Changes Cellular Dynamics**

(A and C) Micrograph sections of day 42 human cerebral organoids electroporated with GFP-empty vector control or human *PLEKHG6* isoform 4 targeting miRNA (miPLEKHG6\_4) and analyzed 7 dpe. Sections were then immunostained for SOX2 (A) or MAP2 (C).

(B and D) Quantification of GFP-expression (GFP<sup>+</sup>) cells transfected with GFP-empty vector alone or miPLEKHG6\_4 that also express (B) SOX2<sup>+</sup> or (D) MAP2 (means  $\pm$  SEMs). Mann-Whitney *U* test; \**p* < 0.05; \*\**p* < 0.01. *n* = 4–6 different organoids per condition from two separate batches. Scale bar represents 30  $\mu$ m.

### Modulation of PLEKHG6 Levels in Cerebral Organoids Induces PH and Is Non-cell Autonomous

PLEKHG6 activates the small GTPase RhoA (Asiedu et al., 2009), a known modulator of neuronal migration and

Given that *PLEKHG6* isoforms 1 and 4 (*PLEKHG6\_1* and *\_4*, respectively) differ only by their first coding exon and that no homology to known signal peptides was detected by Signal-BLAST (Frank and Sippl, 2008) within the N termini encoded by these unique exons, we hypothesized that differential expression is the essential distinguishing feature between these two proteins. To study this, we compared *PLEKHG6\_1* and *PLEKHG6\_4* expression in developing human cortices, specifically in apical and basal radial glia and migrating neurons at 12–13 weeks post-conception (pcw) (Florio et al., 2015). Consistent with differential expression patterns distinguishing the two isoforms, these data recorded *PLEKHG6\_1* as being expressed in migrating neurons and *PLEKHG6\_4* in apical and basal radial glia cells (Figure S2B). An overall greater trend for increased *PLEKHG6* expression is also observed in human radial glia compared to mice, further suggesting an evolutionary link (Figure S2A) (Florio et al., 2015). Using validated polyclonal antibodies that recognize the unique N termini of *PLEKHG6\_1* and *PLEKHG6\_4* (Figure S2C), we further assessed for differential regulation of these two isoforms by immunostaining human cerebral organoids. Consistent with the transcriptomic data, *PLEKHG6\_1* is expressed in post-mitotic neurons (PCNA<sup>−</sup> MAP2<sup>+</sup>), while *PLEKHG6\_4* was present in both proliferating neural progenitors (PCNA<sup>+</sup> MAP2<sup>−</sup>) and neurons (Figures S2D and S2E). To further assess the potential for differential expression among the two isoforms, we analyzed histone signatures (histone H3 lysine 4 tri- and monomethylation) and identified distinct presumptive promoters for *PLEKHG6\_1* and *PLEKHG6\_4* (Rosenbloom et al., 2013), which also correlated with enhanced DNase hypersensitivity (Figure S3). Chromatin immunoprecipitation sequencing (ChIP-seq) data (Rosenbloom et al., 2013) define a mutually exclusive set of transcription factors that also locate differentially at the two *cis*-regulatory elements for these isoforms in non-overlapping cell types (Figure S3). These independent lines of evidence support the differential regulation and expression of *PLEKHG6\_1* and *PLEKHG6\_4*.

cortical development in mice (Cappello et al., 2012). Conditional depletion of RhoA within the developing mouse forebrain is associated with cellular heterotopia; its knockdown *in utero* increases the proportion of electroporated cells at more basal positions along the cortical plate (Cappello et al., 2012). Such differences in phenotype have been linked to the number of cells disrupted using each strategy (Cappello et al., 2012). Thus, while nullizygosity for the primate-specific isoform of *PLEKHG6* (*PLEKHG6\_4*) potentially contributes to the pathogenesis of PH (and if the mechanism is mediated via RhoA), its knockdown within developing organoid cultures would not induce heterotopic cells lining the ventricle but instead increase the number of electroporated cells at the cortical plate. Targeted *PLEKHG6\_4* knockdown in organoid cultures induced changes in the cellular composition of GFP<sup>+</sup> cells 7 days post-electroporation (dpe), with an increased fraction of GFP<sup>+</sup> cells that were also positive for the neuronal marker MAP2 and decreased for the progenitor marker SOX2 (Figures 2 and S4).

The primate-specific isoform of *PLEKHG6* (*PLEKHG6\_4*) is lowly expressed in developing human cortical and cerebral organoid tissue (Camp et al., 2015; Florio et al., 2015). To further explore *PLEKHG6\_4* in human brain development, we next assessed the consequences of misregulation of *PLEKHG6\_4* expression by increasing its levels in organoids via electroporation. Here, ectopic neurons (marked by NeuN) were identified at the ventricular surfaces of organoids at a higher frequency after *PLEKHG6\_4* misregulation compared to controls (Figures 3A and 3B). Notably, these ectopic NeuN<sup>+</sup> cells were GFP<sup>−</sup>, indicating that their heterotopic positioning resulted from a non-cell autonomous mechanism induced by *PLEKHG6\_4* overexpression (Figures 3A and 3B). Associated anomalies observed after electroporation of the *PLEKHG6\_4* construct also included progressive disruption of the neuroepithelial lining and defective apical junction assembly (Figures 3C, 3D, and S5). Specifically, control organoids had a fine

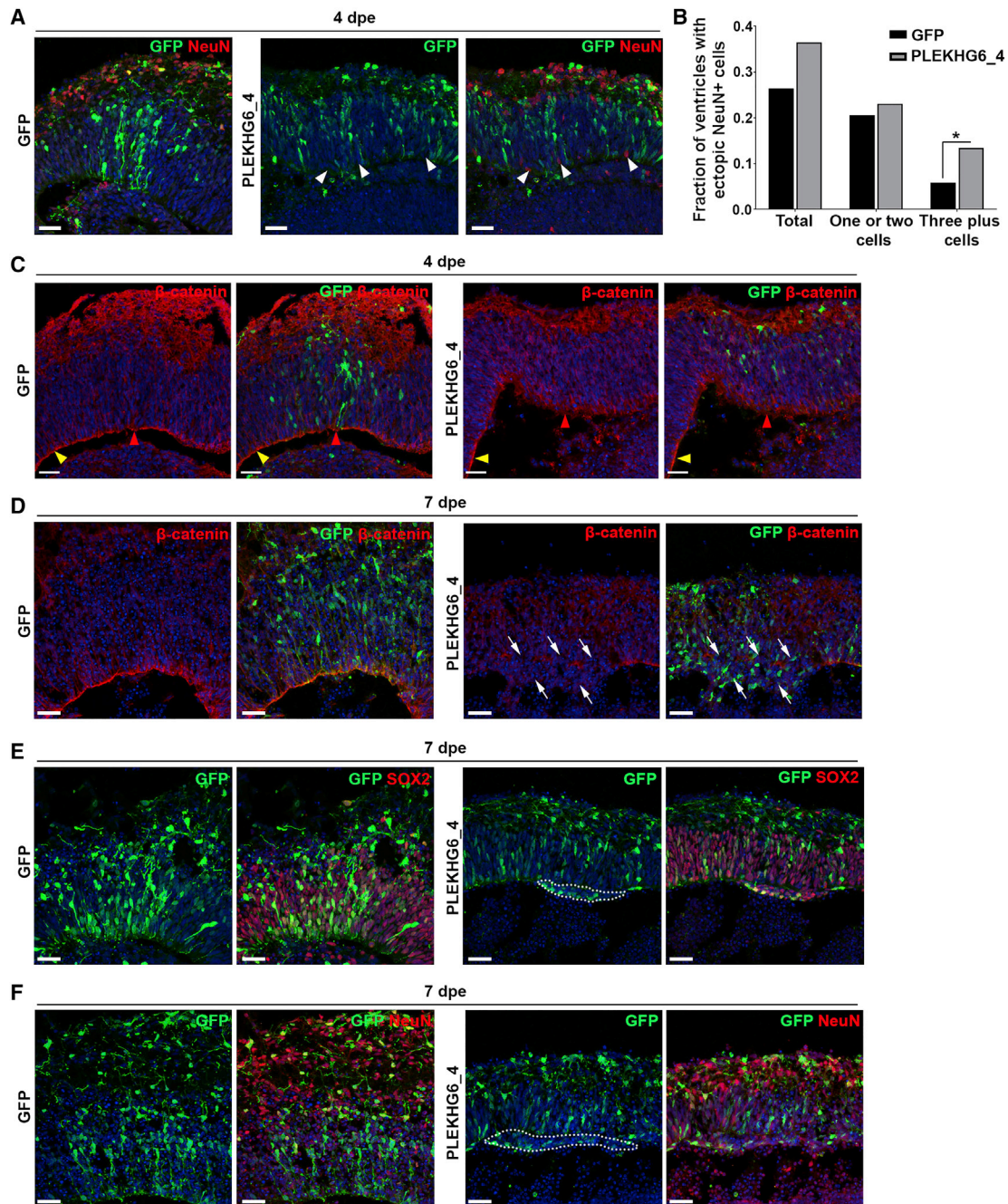


**Figure 3. PLEKHG6\_4 Dysregulation in Human Cerebral Organoids Impairs Ventricular Surface Integrity and Induces PH Formation**

Micrograph sections of day 42 human cerebral organoids electroporated with GFP-empty vector control or human *PLEKHG6* isoform 4 (*PLEKHG6\_4*) and analyzed 4 or 7 dpe. Sections were then immunostained for NeuN,  $\beta$ -catenin, or SOX2, as indicated.

(A) White arrowheads indicate NeuN<sup>+</sup>GFP<sup>−</sup> cells ectopically located directly adjacent to the ventricular surface within the electroporated zone.

(B) Quantification of the percentage of ventricles with ectopic NeuN<sup>+</sup> cells transfected with GFP-empty vector control or human *PLEKHG6\_4* in (A).

(C) Red and yellow arrowheads indicate the  $\beta$ -catenin profile at the electroporated and adjacent non-electroporated ventricular surfaces, respectively.

(D) White arrows indicate heterotopic cells.

(E and F) Dotted lines indicate heterotopic cells.

Exact binomial test; \* $p < 0.05$ .  $n = 4$ –6 different organoids per condition from 2 separate batches. Scale bar represents 30  $\mu$ m.



adherent junction belt along the ventricular surface, staining strongly for  $\beta$ -catenin, phalloidin, and PALS1. This structure was significantly disrupted in organoids overexpressing *PLEKHG6\_4*, with its constituent proteins more diffusely dispersed (Figures 3C, 3D, and S5). The heterotopic neurons clustering at the ventricular surface 7 dpe formed PH-like nodules composed of neural progenitors (marked by SOX2) and NeuN<sup>+</sup> neurons (Figures 3E and 3F). Thus, modulation of *PLEKHG6\_4* activity within human cerebral organoids demonstrates a role for this factor in neurogenesis and reproduces features of PH.

### Forced *PLEKHG6\_4* Expression within Apical Progenitors of the Developing Mouse Cortex Promotes Non-cell Autonomous Expansion of Basal Progenitors

Given that *PLEKHG6\_4* represents a newly evolved feature of the primate coding genome, we next assessed the effects of forced expression of this isoform during neurogenesis. To this end, we overexpressed this isoform in the developing mouse cortex by *in utero* electroporation on embryonic day 13 (E13). Analysis 3 dpe (E16) demonstrated that forced expression of *PLEKHG6\_4* decreased the proportion of GFP<sup>+</sup> cells in the VZ and increased their numbers in the inner cortical plate (CP1) relative to vector-only control cortices (Figures 4A and 4B;  $p < 0.05$ ). The proportion of GFP<sup>+</sup> cells expressing Pax6 in cortices expressing *PLEKHG6\_4* was reduced relative to controls (Figures 4C and 4D). However, a significant 4-fold expansion of basally located (Tbr2<sup>+</sup>) progenitors relative to controls was observed after *PLEKHG6\_4* forced expression (Figures 4E and 4G). We were surprised to find that these basal progenitors were not GFP<sup>+</sup> (Figures 4E and 4F), indicating that, as also observed in human cerebral organoids, a non-cell autonomous mechanism underlies this observation. Increased numbers of Tbr1<sup>+</sup>GFP<sup>+</sup> neuronal cells were also observed within developing cortices overexpressing *PLEKHG6\_4* (Figures 4H and 4I), although this observation is unlikely to be due to a direct effect, as *PLEKHG6\_4* overexpression in primary mouse cortices isolated at E13 and cultured *in vitro* did not significantly increase the number of neurons ( $\beta$ -III tubulin<sup>+</sup>), even after 5 days of differentiation (data not shown). Similar to the organoid data, we detected a disruption in the neuroepithelial lining within the electroporated region (Figure 4J). Developing cortices electroporated with *PLEKHG6\_4* expressing constructs also induce radial glial cells to lose their radial morphology (Figure S6). These data show that forced expression of *PLEKHG6\_4* in apical progenitors enhances the production of neurons and basal progenitor production, the latter effect most likely through non-cell autonomous mechanisms.

### *Plekhg6* Is a Regulator of Neurogenesis and Neuronal Migration in the Developing Mouse Brain

To better understand the mechanism leading to the defects noted after modulation of *PLEKHG6\_4*, we next evaluated the phenotypic effects induced after knockdown of *Plekhg6* in developing mouse cortices. To explore whether reduced *Plekhg6* levels also modulate neurogenesis, as they did in the organoid model, we introduced a bi-cistronic vector ex-

pressing GFP and validated microRNAs (miRNAs) directed against *Plekhg6* (Figures S7A–S7C) into the ventricular neuroepithelium of E13 embryos using *in utero* electroporation. As for *PLEKHG6\_4* knockdown in organoids (and consistent with the RhoA knockdown phenotype observed previously [Cappello et al., 2012]), *Plekhg6* knockdown induced changes in the cellular distribution of GFP<sup>+</sup> cells 3 dpe (E16) with an increased fraction of GFP<sup>+</sup> in the outer cortical plate (CP2) relative to vector-only control cortices (Figures 5C and 5D;  $p < 0.01$ , Figures S7A and S7C). In addition, we observed an overmigration of neurons that breached the basement membrane in five of the seven developing cortices subject to *Plekhg6* knockdown (Figure 6A). A similar effect was observed after acute knockdown of RhoA (Cappello et al., 2012). Both GFP<sup>+</sup>Pax6<sup>+</sup> apical and GFP<sup>+</sup>Tbr2<sup>+</sup> basal progenitors were correspondingly depleted in miRNA-treated cortices relative to the vector-only control (Figures 5E, 5G, 5I, and 5K). Mitotically active phosphorylated histone H3 (pH3<sup>+</sup>) cells positive for GFP were also depleted 3 dpe (Figures 5F and 5J), while an increase in the number of GFP cells positive for the early neuronal marker Tbr1 was observed (Figures 5H and 5L). These differences were not evident at an earlier time point (1 dpe; Figures 5E–5L), despite a significant increase in GFP<sup>+</sup> cells expressing the miRNA within the upper cortical plate (Figures 5A and 5B). These observations were not explained by changes in cell death as ascertained by the measurement of activated caspase 3 (Figures S7D and S7E). These data support a role for *Plekhg6* in influencing both neuroprogenitor differentiation and neuronal migration.

### Knockdown of *Plekhg6* Mediates Changes in Neuronal Migration via RhoA that Can Be Rescued by Human *PLEKHG6\_4*

To directly test whether modulation of RhoA activity can explain the redistribution of neurons after knockdown of *Plekhg6*, we co-electroporated a constitutively activated (“fast cycling”) mutant of RhoA with the miRNA against *Plekhg6* (Figures 6B and 6C). This active form of RhoA rescued the neuronal mispositioning that was observed after *Plekhg6* knockdown (Figures 6B and 6C).

With only 6% of the protein sequence differing between *PLEKHG6\_1* and *PLEKHG6\_4* and no homology to known signal peptides within the N terminus encoded by the unique first exon of *PLEKHG6\_4*, we further hypothesized that both isoforms have the same RhoA catalytic function. Consistent with this scenario, overexpression of human *PLEKHG6\_4* within E13 mouse cortices rescued the altered neuronal distribution observed after knockdown of *Plekhg6* (Figures 6D and 6E). Further confirming functional equivalence between *PLEKHG6\_4* and *Plekhg6*, a RhoA/Rho kinase-based cell transfection assay demonstrated comparable RhoGTPase activity between *PLEKHG6\_1* and *PLEKHG6\_4* and a truncated *PLEKHG6* isoform (*PLEKHG6\_744*) containing only the sequence in common between these two versions (Figures 6F–6H). These data indicate that the different N termini of each *PLEKHG6* isoform do not influence its catalytic function as a modulator of RhoA activity and suggest that it is the differential expression patterns of these two isoforms (Figures S2 and S3) that distinguish them from each other.

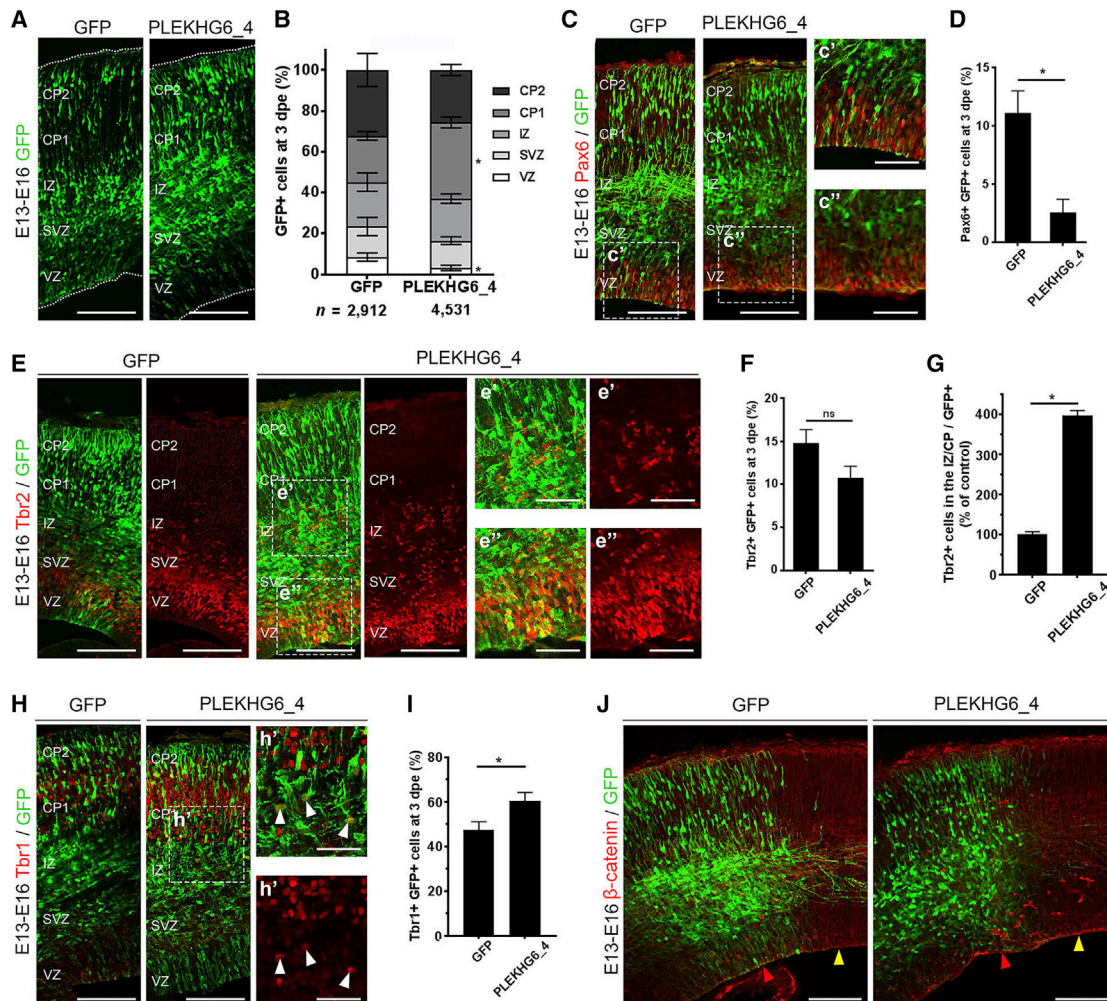


**Figure 4. PLEKHG6\_4 Overexpression Disrupts VZ Integrity and Induces Basal Progenitor Cell Expansion in the Developing Mouse Cortex**

(A) Coronal micrograph sections of E16 mouse cerebral cortices electroporated at E13 with GFP-empty vector control or human *PLEKHG6* isoform 4 (*PLEKHG6\_4*) and analyzed 3 dpe.

(B) Quantification of the distribution of GFP-expressing (GFP<sup>+</sup>) cells transfected with the various constructs in (A).

(C–I) Coronal micrograph sections of the cerebral cortex electroporated with GFP-empty vector control or *PLEKHG6\_4* at E13 with immunostaining at E16 (3 dpe) for Pax6 (C), Tbr2 (E), or Tbr1 (H). (D, F, G, and I) Electroporated GFP<sup>+</sup> cells co-stained for their respective markers were counted over a representative cross-sectional area of the cerebral cortex and presented graphically (means ± SEMs). (H) White arrowheads indicate cells staining for the indicated markers and GFP. (J) Coronal micrograph sections of the cerebral cortex electroporated with GFP-empty vector control or *PLEKHG6\_4* at E13 with immunostaining at E16 (3 dpe) for β-catenin. Red and yellow arrowheads indicate the disposition of β-catenin at the electroporated and adjacent non-electroporated ventricular surfaces, respectively.

For (A), the cortex was subdivided into five equally thick bins approximately corresponding to VZ (bin 1), SVZ (bin 2), IZ (bin 3), and CP (bins 4 and 5). IZ, intermediate zone; SVZ, subventricular zone. Four to six embryos were analyzed for each condition. n, total number of GFP<sup>+</sup> cells counted per condition. Mann-Whitney *U* test; \**p* < 0.05; ns, not significant. Scale bar represents 100 μm (A), (C), (E), (H), and (J); 50 μm (c'), (c''), (e'), (e''), (h'), and (h'').

## DISCUSSION

### The Emerging Role of bRG Dysfunction in PH and Neurodevelopmental Disease

This study has outlined a significant link between genes with *de novo* variants detected in patients with PH and the transcriptional networks present in human basal progenitor cells, specifically bRG. The paucity of *de novo* variants in genes correlating with apical progenitor cell fate suggests that it is the functional impairment of the basal progenitor population that is important

in the pathogenesis of at least some cases of PH. Dysfunction of bRG may also be of broad significance for the pathogenesis of many neurodevelopmental disorders. For example, examination of a cerebral organoid model for classical lissencephaly, a structural malformation of cortical development characterized by the absence of folds (i.e., gyri and sulci), highlighted delayed mitosis specifically in bRG as one of the critical cellular defects leading to this condition (Bershteyn et al., 2017). More widely, an overrepresentation of variants in patients with autism spectrum disorders (ASDs) was also observed in loci demonstrating



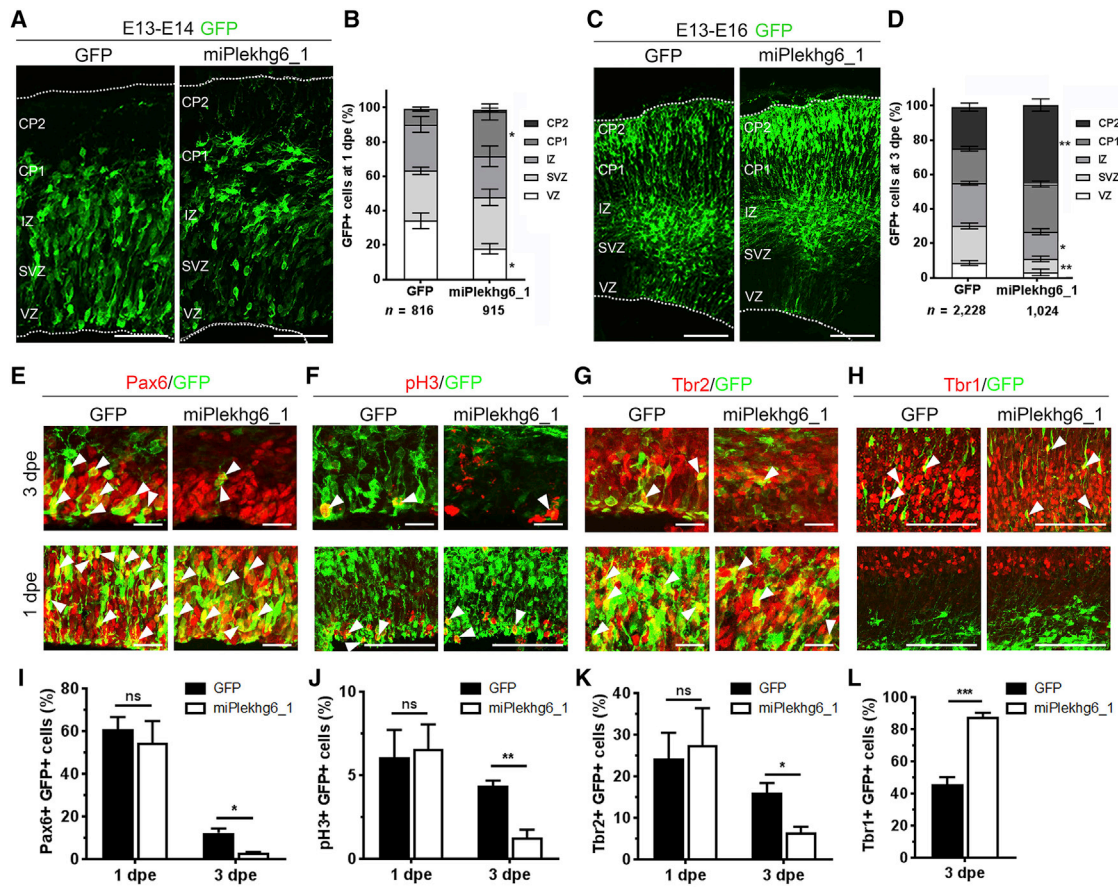


**Figure 5. *Plekhg6* Knockdown Disrupts Neuroprogenitor Differentiation and Neuronal Migration in the Developing Mouse Cortex**

(A–D) Coronal micrograph sections of E14 (A) and E16 (C) mouse cerebral cortices electroporated at E13 with GFP-empty vector control or *Plekhg6* targeting miRNAs (miPlekhg6\_1). Quantification of the distribution of GFP-expression (GFP<sup>+</sup>) cells transfected with GFP-empty vector alone or *Plekhg6* miRNAs 1 dpe (B) and 3 dpe (D) (means ± SEMs).

(E–H) Coronal micrograph sections of the cerebral cortex electroporated with GFP-empty vector control or *Plekhg6* miRNAs (miPlekhg6\_1) at E13 with immunostaining at E14 (1 dpe) or E16 (3 dpe) for Pax6 (E), pH3 (F), Tbr2 (G), or Tbr1 (H).

(I–L) Electroporated GFP<sup>+</sup> cells co-stained for their respective markers were counted over a representative cross-sectional area of the cerebral cortex and presented graphically (means ± SEMs).

White arrowheads indicate cells staining for the indicated markers and expressing GFP. For (A) and (C), the cortex was subdivided into five equally thick bins approximately corresponding to VZ (bin 1), SVZ (bin 2), IZ (bin 3), and CP (bins 4 and 5). Five and seven embryos were analyzed for the 1 and 3 dpe cortices, respectively. n, total number of GFP<sup>+</sup> cells counted per condition. Mann-Whitney *U* test; \**p* < 0.05; \*\**p* < 0.01; \*\*\**p* < 0.001; ns, not significant. Scale bar represents (A) 50 μm; (C) 100 μm; (E)–(G) 20 μm; and (F) and (H) 100 μm.

accelerated divergence between humans and other species (called human accelerated regions) (Doan et al., 2016). Such associations support the suggestion that an evolutionary trade-off has occurred between recent primate brain complexification and a susceptibility of humans to the development of neurodevelopmental and neuropsychiatric conditions.

#### Dysregulation of PLEKHG6 Isoform 4 Regulates Neurogenesis and Neuronal Migration via RhoA

Extending the hypothesis that variants in genes that have recently acquired functions in the brain may contribute to the formation of PH, we identified two variants in *ABAT* and *PLEKHG6* as candidates for further functional validation. Focusing on *PLEKHG6*, a role for a primate-specific isoform in regulating neurogenesis and neuron positioning within the developing cortex

was identified. PLEKHG6 activates the small GTPase RhoA (Asiedu et al., 2009), a known modulator of neuronal migration, whose conditional depletion within the developing mouse forebrain is associated with heterotopically positioned neurons along the ventricular margin (Cappello et al., 2012). In addition to variants in *PLEKHG6* being under intense purifying selection, these data place this gene in a cellular context, the dysfunction of which has been previously implicated in the generation of this disease phenotype. Patients with deleterious variants in this gene (or its differential *cis*-regulatory elements) will further consolidate this proposed mechanism. In testing this hypothesis, we identified multiple parallels between the consequences of misregulation of *PLEKHG6* with those that are observed after the modulation of RhoA activity (Cappello et al., 2012). First, increases in both *PLEKHG6* and *RhoA* expression (Cappello

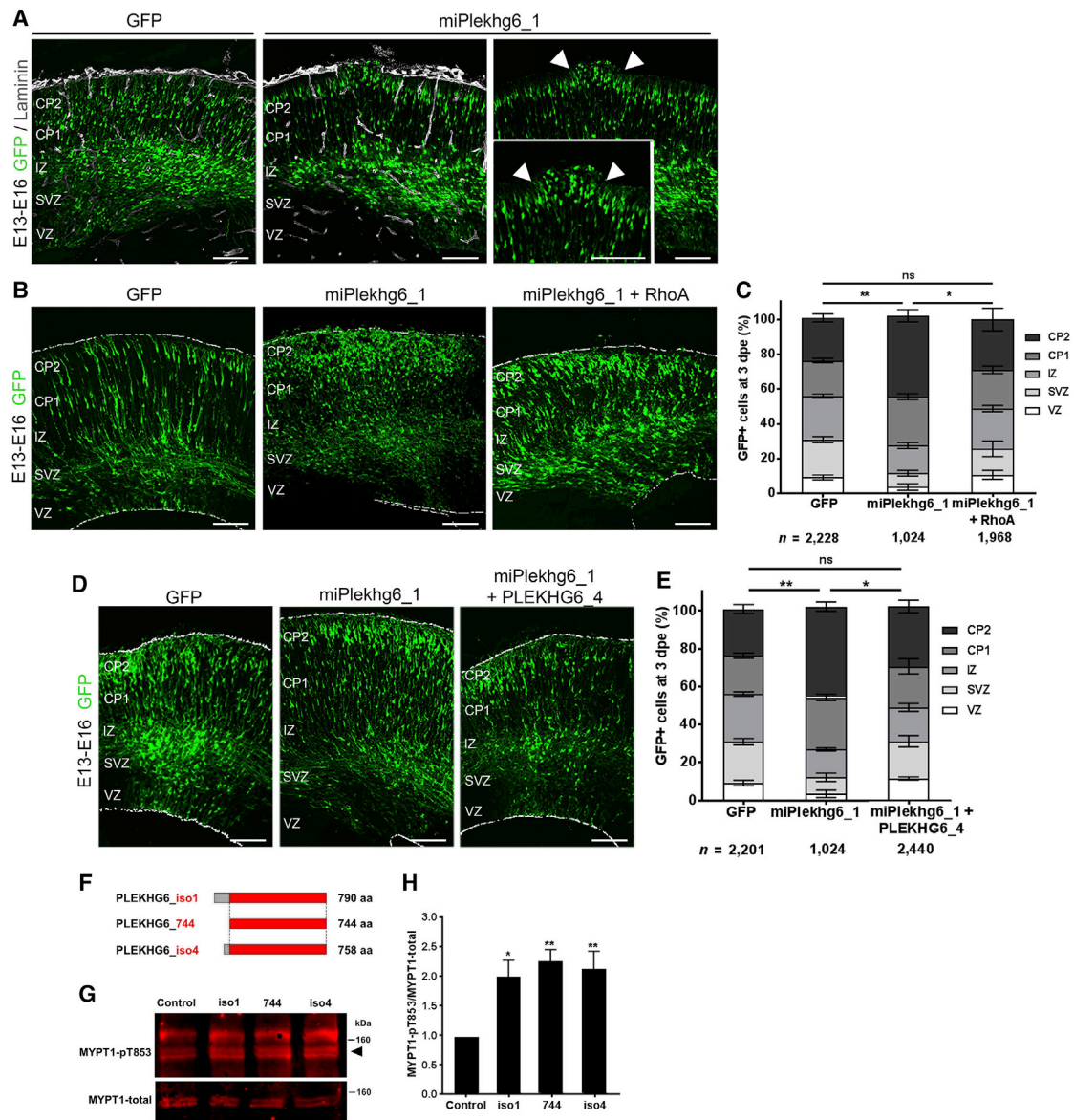


**Figure 6. Plekhg6 Regulates RhoA to Facilitate Neuronal Migration in the Developing Mouse Cortex**

(A) Coronal micrograph sections of E16 mouse cerebral cortices electroporated with GFP-empty vector control or *Plekhg6* miRNAs (miPlekhg6\_1) and stained for laminin. White arrowheads indicate the overmigration phenotype evident at the pial surface of the cortex.

(B) Coronal micrograph sections of E16 mouse cerebral cortices electroporated with GFP-empty vector control, *Plekhg6* miRNAs (miPlekhg6\_1), or miPlekhg6\_1, together with a construct encoding a fast-cycling form of RhoA.

(C) Quantification of the distribution of GFP-expressing (GFP<sup>+</sup>) cells transfected with the various constructs in (B).

(D) Coronal micrograph sections of E16 mouse cerebral cortices electroporated at E13 with GFP-empty vector control, *Plekhg6* miRNA (miPlekhg6\_1), or miPlekhg6\_1, together with the miRNA-resistant human *PLEKHG6* isoform 4 (PLEKHG6\_4).

(E) Quantification of the distribution of GFP-expressing (GFP<sup>+</sup>) cells transfected with the various constructs in (D).

(F) Domain structure of PLEKHG6\_1, truncated PLEKHG6 (PLEKHG6\_744), and PLEKHG6\_4. Red, common sequence; gray, unique sequences across the two isoforms.

(G) Immunoblot showing Rho-guanine nucleotide exchange factor (GEF) activity of myc-tagged PLEKHG6 isoform 1 (PLEKHG6\_iso1), truncated PLEKHG6 (PLEKHG6\_744), and PLEKHG6 isoform 4 (PLEKHG6\_iso4), as determined by dephosphorylation of myosin phosphatase target protein 1 (MYPT1-pT853). The arrowhead denotes MYPT1.

(H) Quantifications representing three biological replicates of (G) summarizing the proportion of phosphorylated MYPT1 at residue 853 relative to total MYPT1 and normalized against the loading control glyceraldehyde 3-phosphate dehydrogenase (GAPDH) in HEK293 cells.

For (B) and (D), the cortex was subdivided into five equally thick bins approximately corresponding to VZ (bin 1), SVZ (bin 2), IZ (bin 3), and CP (bins 4 and 5). Five embryos were analyzed for each condition. n, total number of GFP<sup>+</sup> cells counted per condition. One-way ANOVA; \*p < 0.05; \*\*p < 0.01; ns, not significant, with reference to cells in CP2. Scale bar represents 100  $\mu$ m.

et al., 2012) within the developing mouse cortex decrease the number of neurons at the CP2. Second, knockdown of either *Plekhhg6* or RhoA within the developing mouse cortex leads to enhanced neuronal migration and even cellular overmigration beyond the cortical plate, forming heterotopic clusters of neurons at the pial surface. Alterations in the radial glial scaffold are also observed after overexpression of *RhoA* or *PLEKHG6\_4*. RhoA rescued the altered neuronal distribution induced by *Plekhhg6* knockdown, with our studies also indicating that the primate-specific version of the *PLEKHG6\_4* gene functionally compensates for a reduction in *Plekhhg6\_1*, and that both isoforms exhibit similar Rho GTPase-activating potential.

Several lines of evidence indicate that RhoA could represent a major signaling mediator facilitating networks associated with brain evolution. Recently, studies examining genetic factors contributing to human cerebral cortex complexification using comparative mouse and human bRG transcriptomic profiling uncovered a novel human-specific RhoA regulator, ARHGAP11B and a further four Rho regulators whose expression was enriched in bRG relative to their apical counterparts (Florio et al., 2015). RhoA is a key determinant for bRG delamination and OSVZ formation through activation of the Rho effector ROCK and non-muscle myosin II (Ostrem et al., 2014). PLEKHG6 also directly binds and regulates non-muscle myosin II activity via RhoA (Wu et al., 2006). Results from the Rho assay described here also show that PLEKHG6 is a regulator of the RhoA-ROCK target protein myosin phosphatase target subunit (MYPT-1), a known modulator of non-muscle myosin II activity (Watanabe et al., 2007).

Although both PLEKHG6\_1 and PLEKHG6\_4 were identified as having the same RhoA catalytic activity, these isoforms differ in their spatial expression patterns (Hawrylycz et al., 2012). Changes in temporal and spatial regulation of RhoA have been well documented in several developmental contexts (Cappello et al., 2012; Herzog et al., 2011; Katayama et al., 2011). For example, conditional depletion of RhoA in the spinal cord or midbrain of developing mouse embryos affects the maintenance of adherens junctions but induces hypoproliferation (in spinal cord) and hyperproliferation (in midbrain) of neural progenitor cells in each tissue (Katayama et al., 2011; Herzog et al., 2011). Although alternative promoter use and splicing are ubiquitous mechanisms of gene regulation in multicellular organisms to create transcriptional diversity, their functional impact on evolutionary expansion of the cerebral cortex and, in particular, basal progenitor function is only beginning to emerge (Pollen et al., 2015; Johnson et al., 2015).

### PLEKHG6 Influences VZ Integrity

Forced expression of *PLEKHG6\_4* within the developing mouse forebrain disrupted the integrity of the ventricular surface, a mechanism that has an established precedent in the pathogenesis of PH (Sheen et al., 2001; Ferland et al., 2009; Caraballona et al., 2012). Recently, a role for adhesion junction belt downregulation at the VZ surface during basal progenitor delamination (Tavano et al., 2018) was shown to be facilitated by *Plekha7*, a paralog of *Plekhhg6*, which also exhibits differential isoform expression. Furthermore, non-cell autonomous basal progenitor expansion was also recently reported upon knockdown of the

chromatin remodeling factor BAF155 (Narayanan et al., 2018). Thus, although the exact underlying mechanism resulting in basal progenitor expansion after *PLEKHG6\_4* overexpression has yet to be fully elucidated, a wider role for this family of proteins and the non-cell autonomous features associated with such events in cortical neurogenesis may be emerging.

Non-cell autonomous mechanisms are increasingly being reported in the context of cortical malformations as experimental model systems emerge that are capable of exploring these functions. For example, in Miller-Dieker syndrome (a severe form of lissencephaly), a recent organoid model identified impairments to apical polarity machinery formation that then disrupt cell-cell N-cadherin/ $\beta$ -catenin signaling within the VZ niche, with resultant defects in cell fate control exerted in a non-cell autonomous fashion (Iefremova et al., 2017). Such changes were also associated with disrupted ventricular surface integrity and a switch from symmetric to asymmetric divisions of aRG that increased the proportion of basal intermediate progenitors, a phenotype comparable to that outlined in the present study. Furthermore, a recent report showed that *ASPM* (a gene whose dysregulation is linked to microcephaly) can regulate aRG cell affinity to the ventricular surface, with contingent effects on the expansion of basal progenitors (bRG and basal intermediate progenitors) (Johnson et al., 2018). This growing body of evidence links ventricular surface integrity and apical cell dynamics with neurodevelopmental disease phenotypes and cortical complexification.

Since bRG cells are proposed to represent the cellular substrate for recent primate neocortical expansion (Fietz et al., 2010; Hansen et al., 2010), a susceptibility to develop PH could be conferred by mutations in recently evolved genomic elements regulating this cell type. The biallelic loss of function of a primate-specific *PLEKHG6* isoform leading to the disruption of neurogenesis in pathways already linked to cellular heterotopia, although present in a single case, could also be illustrative of a wider theme of variants in recently evolved genomic elements leading to developmental disorders (Doan et al., 2016). Such a result has significant implications for the functional study of this and other neurodevelopmental disorders and could explain why mice models frequently do not recapitulate phenotypes relating to basal progenitor cellular dysfunction (Feng et al., 2006; Hart et al., 2006; Corbo et al., 2002). We anticipate that evolutionarily dynamic non-coding sequences (Vermunt et al., 2016) will harbor similar genomic innovations that can be linked to neurodevelopmental disease in humans. Where the genetic substrate for such functions is not present in the genome of mammals typically used to model neurodevelopmental conditions (e.g., mice), studies of individuals with neurodevelopmental disorders such as PH can direct attention to key regions of the genome that may contribute to cortical complexification in humans.

### STAR★METHODS

Detailed methods are provided in the online version of this paper and include the following:

- KEY RESOURCES TABLE
- CONTACT FOR REAGENT AND RESOURCE SHARING



- **EXPERIMENTAL MODEL AND SUBJECT DETAILS**
  - PH Trios
  - iPSC generation and human organoids
  - Mice
- **METHOD DETAILS**
  - Whole-exome sequencing
  - Whole-exome sequencing variant calling
  - Burden analysis
- **QUANTIFICATION AND STATISTICAL ANALYSIS**

## SUPPLEMENTAL INFORMATION

Supplemental Information includes four tables and seven figures and can be found with this article online at <https://doi.org/10.1016/j.celrep.2018.11.029>.

## ACKNOWLEDGMENTS

We thank the families for their participation in this study. The Exome Aggregation Consortium is acknowledged for access to data, as are Marta Florio and Wieland Huttner for the investigation of *PLEKHG6* isoform expression in fetal tissue. The authors also thank Kalina Draganova for insightful feedback on the manuscript. R.G. is supported by funding from the European Union through the Seventh Framework Programme (FP7) under the project DESIRE (N602531). M.G. is supported by funding from the European Research Council (ERC) grant ChroNeuroRepair. S.P.R. is supported by funding from the Health Research Council of New Zealand and Cure Kids NZ. S.C. is supported by funding from the German Research Foundation grant CA 1205/2-1. A.C.O. was supported by a grant from the Deutschcher Akademischer Austauschdienst of the German Research Council, a University of Otago Postgraduate Scholarship Award, and a Philip Wrightson Postdoctoral Fellowship from the Neurological Foundation of New Zealand.

## AUTHOR CONTRIBUTIONS

Conceptualization, A.C.O., S.C., and S.P.R.; Methodology, A.C.O., C.K., and J.K.; Software, A.C.O. and D.M.M.; Investigation, A.C.O., C.K., T.M., and Z.A.J.; Writing – Original Draft, A.C.O.; Funding Acquisition, M.G., S.C., and S.P.R.; Resources, M.G., M.D., R.J.L., E.P.K., A.F., D.T.P., S.F.B., I.E.S., and R.G.; Supervision, S.C. and S.P.R. All of the authors contributed to the final review and edits of the manuscript.

## DECLARATION OF INTERESTS

The authors declare no competing interests.

Received: March 26, 2018

Revised: September 6, 2018

Accepted: November 5, 2018

Published: December 4, 2018

## REFERENCES

Asiedu, M., Wu, D., Matsumura, F., and Wei, Q. (2009). Centrosome/spindle pole-associated protein regulates cytokinesis via promoting the recruitment of MyoGEF to the central spindle. *Mol. Biol. Cell* 20, 1428–1440.

Auton, A., Brooks, L.D., Durbin, R.M., Garrison, E.P., Kang, H.M., Korbel, J.O., Marchini, J.L., McCarthy, S., McVean, G.A., and Abecasis, G.R.; 1000 Genomes Project Consortium (2015). A global reference for human genetic variation. *Nature* 526, 68–74.

Bae, B.I., Tietjen, I., Atabay, K.D., Evrony, G.D., Johnson, M.B., Asare, E., Wang, P.P., Murayama, A.Y., Im, K., Lisgo, S.N., et al. (2014). Evolutionarily dynamic alternative splicing of GPR56 regulates regional cerebral cortical patterning. *Science* 343, 764–768.

Bayés, A., van de Lagemaat, L.N., Collins, M.O., Croning, M.D., Whittle, I.R., Choudhary, J.S., and Grant, S.G. (2011). Characterization of the proteome,

diseases and evolution of the human postsynaptic density. *Nat. Neurosci.* 14, 19–21.

Bershteyn, M., Nowakowski, T.J., Pollen, A.A., Di Lullo, E., Nene, A., Wynshaw-Boris, A., and Kriegstein, A.R. (2017). Human iPSC-derived cerebral organoids model cellular features of lissencephaly and reveal prolonged mitosis of outer radial glia. *Cell Stem Cell* 20, 435–449.e4.

Betizeau, M., Cortay, V., Patti, D., Pfister, S., Gautier, E., Bellemin-Ménard, A., Afanassieff, M., Huisoud, C., Douglas, R.J., Kennedy, H., and Dehay, C. (2013). Precursor diversity and complexity of lineage relationships in the outer subventricular zone of the primate. *Neuron* 80, 442–457.

Blake, J.A., Bult, C.J., Kadin, J.A., Richardson, J.E., and Eppig, J.T.; Mouse Genome Database Group (2011). The Mouse Genome Database (MGD): premier model organism resource for mammalian genomics and genetics. *Nucleic Acids Res.* 39, D842–D848.

Borrell, V., and Götz, M. (2014). Role of radial glial cells in cerebral cortex folding. *Curr. Opin. Neurobiol.* 27, 39–46.

Borrell, V., and Reillo, I. (2012). Emerging roles of neural stem cells in cerebral cortex development and evolution. *Dev. Neurobiol.* 72, 955–971.

Camp, J.G., Badsha, F., Florio, M., Kanton, S., Gerber, T., Wilsch-Bräuninger, M., Lewitus, E., Sykes, A., Hevers, W., Lancaster, M., et al. (2015). Human cerebral organoids recapitulate gene expression programs of fetal neocortex development. *Proc. Natl. Acad. Sci. USA* 112, 15672–15677.

Cappello, S., Böhringer, C.R., Bergami, M., Conzelmann, K.K., Ghanem, A., Tomassy, G.S., Ariotta, P., Mainardi, M., Allegra, M., Caleo, M., et al. (2012). A radial glia-specific role of RhoA in double cortex formation. *Neuron* 73, 911–924.

Cappello, S., Gray, M.J., Badouel, C., Lange, S., Einsiedler, M., Srouf, M., Chitayat, D., Hamdan, F.F., Jenkins, Z.A., Morgan, T., et al. (2013). Mutations in genes encoding the cadherin receptor-ligand pair DCHS1 and FAT4 disrupt cerebral cortical development. *Nat. Genet.* 45, 1300–1308.

Caraballona, A., Beguin, S., Pallesi-Pocachard, E., Buhler, E., Pellegrino, C., Arnaud, K., Hubert, P., Oualha, M., Siffroi, J.P., Khantane, S., et al. (2012). A glial origin for periventricular nodular heterotopia caused by impaired expression of Filamin-A. *Hum. Mol. Genet.* 21, 1004–1017.

Corbo, J.C., Deuel, T.A., Long, J.M., LaPorte, P., Tsai, E., Wynshaw-Boris, A., and Walsh, C.A. (2002). Doublecortin is required in mice for lamination of the hippocampus but not the neocortex. *J. Neurosci.* 22, 7548–7557.

Darnell, J.C., Van Driesche, S.J., Zhang, C., Hung, K.Y., Mele, A., Fraser, C.E., Stone, E.F., Chen, C., Fak, J.J., Chi, J.J., et al. (2011). FMRP stalls ribosomal translocation on mRNAs linked to synaptic function and autism. *Cell* 146, 247–261.

DePristo, M.A., Banks, E., Poplin, R., Garimella, K.V., Maguire, J.R., Hartl, C., Philippakis, A.A., del Angel, G., Rivas, M.A., Hanna, M., et al. (2011). A framework for variation discovery and genotyping using next-generation DNA sequencing data. *Nat. Genet.* 43, 491–498.

Doan, R.N., Bae, B.I., Cubelos, B., Chang, C., Hossain, A.A., Al-Saad, S., Mukaddes, N.M., Oner, O., Al-Saffar, M., Balkhy, S., et al. (2016). Mutations in human accelerated regions disrupt cognition and social behavior. *Cell* 167, 341–354.e12.

Feldman, I., Rzhetsky, A., and Vitkup, D. (2008). Network properties of genes harboring inherited disease mutations. *Proc. Natl. Acad. Sci. USA* 105, 4323–4328.

Feng, Y., Chen, M.H., Moskowitz, I.P., Mendonza, A.M., Vidali, L., Nakamura, F., Kwiatkowski, D.J., and Walsh, C.A. (2006). Filamin A (FLNA) is required for cell-cell contact in vascular development and cardiac morphogenesis. *Proc. Natl. Acad. Sci. USA* 103, 19836–19841.

Ferland, R.J., Batiz, L.F., Neal, J., Lian, G., Bundock, E., Lu, J., Hsiao, Y.C., Diamond, R., Mei, D., Banham, A.H., et al. (2009). Disruption of neural progenitors along the ventricular and subventricular zones in periventricular heterotopia. *Hum. Mol. Genet.* 18, 497–516.

Fietz, S.A., Kelava, I., Vogt, J., Wilsch-Bräuninger, M., Stenzel, D., Fish, J.L., Corbeil, D., Riehn, A., Distler, W., Nitsch, R., and Huttner, W.B. (2010).



- OSVZ progenitors of human and ferret neocortex are epithelial-like and expand by integrin signaling. *Nat. Neurosci.* **13**, 690–699.
- Florio, M., Albert, M., Taverna, E., Namba, T., Brandl, H., Lewitus, E., Haffner, C., Sykes, A., Wong, F.K., Peters, J., et al. (2015). Human-specific gene ARHGAP11B promotes basal progenitor amplification and neocortex expansion. *Science* **347**, 1465–1470.
- Frank, K., and Sippl, M.J. (2008). High-performance signal peptide prediction based on sequence alignment techniques. *Bioinformatics* **24**, 2172–2176.
- Guerrini, R., and Dobyns, W.B. (2014). Malformations of cortical development: clinical features and genetic causes. *Lancet Neurol.* **13**, 710–726.
- Hansen, D.V., Lui, J.H., Parker, P.R., and Kriegstein, A.R. (2010). Neurogenic radial glia in the outer subventricular zone of human neocortex. *Nature* **464**, 554–561.
- Hart, A.W., Morgan, J.E., Schneider, J., West, K., McKie, L., Bhattacharya, S., Jackson, I.J., and Cross, S.H. (2006). Cardiac malformations and midline skeletal defects in mice lacking filamin A. *Hum. Mol. Genet.* **15**, 2457–2467.
- Haubensak, W., Attardo, A., Denk, W., and Huttner, W.B. (2004). Neurons arise in the basal neuroepithelium of the early mammalian telencephalon: a major site of neurogenesis. *Proc. Natl. Acad. Sci. USA* **101**, 3196–3201.
- Hawrylycz, M.J., Lein, E.S., Guillozet-Bongaarts, A.L., Shen, E.H., Ng, L., Miller, J.A., van de Lagemaat, L.N., Smith, K.A., Ebbert, A., Riley, Z.L., et al. (2012). An anatomically comprehensive atlas of the adult human brain transcriptome. *Nature* **489**, 391–399.
- Heinzen, E.L., O'Neill, A.C., Zhu, X., Allen, A.S., Bahlo, M., Chelly, J., Chen, M.H., Dobyns, W.B., Freytag, S., Guerrini, R., et al.; Epi4K Consortium; Epilepsy Phenome/Genome Project (2018). De novo and inherited private variants in MAP1B in periventricular nodular heterotopia. *PLoS Genet.* **14**, e1007281.
- Herzog, D., Loetscher, P., van Hengel, J., Knüsel, S., Brakebusch, C., Taylor, V., Suter, U., and Relvas, J.B. (2011). The small GTPase RhoA is required to maintain spinal cord neuroepithelium organization and the neural stem cell pool. *J. Neurosci.* **31**, 5120–5130.
- Huang, N., Lee, I., Marcotte, E.M., and Hurler, M.E. (2010). Characterising and predicting haploinsufficiency in the human genome. *PLoS Genet.* **6**, e1001154.
- Iefremova, V., Manikakis, G., Krefft, O., Jabali, A., Weynans, K., Wilkens, R., Marsoner, F., Brändl, B., Müller, F.J., Koch, P., and Ladewig, J. (2017). An organoid-based model of cortical development identifies non-cell-autonomous defects in Wnt signaling contributing to Miller-Dieker syndrome. *Cell Rep.* **19**, 50–59.
- Iossifov, I., Ronemus, M., Levy, D., Wang, Z., Hakker, I., Rosenbaum, J., Yamrom, B., Lee, Y.H., Narzisi, G., Leotta, A., et al. (2012). De novo gene disruptions in children on the autistic spectrum. *Neuron* **74**, 285–299.
- Iossifov, I., O'Roak, B.J., Sanders, S.J., Ronemus, M., Krumm, N., Levy, D., Stessman, H.A., Witherspoon, K.T., Vives, L., Patterson, K.E., et al. (2014). The contribution of de novo coding mutations to autism spectrum disorder. *Nature* **515**, 216–221.
- Johnson, M.B., Wang, P.P., Atabay, K.D., Murphy, E.A., Doan, R.N., Hecht, J.L., and Walsh, C.A. (2015). Single-cell analysis reveals transcriptional heterogeneity of neural progenitors in human cortex. *Nat. Neurosci.* **18**, 637–646.
- Johnson, M.B., Sun, X., Kodani, A., Borges-Monroy, R., Girsakis, K.M., Ryu, S.C., Wang, P.P., Patel, K., Gonzalez, D.M., Woo, Y.M., et al. (2018). Aspm knockout ferret reveals an evolutionary mechanism governing cerebral cortical size. *Nature* **556**, 370–375.
- Kang, H.J., Kawasawa, Y.I., Cheng, F., Zhu, Y., Xu, X., Li, M., Sousa, A.M., Pletikos, M., Meyer, K.A., Sedmak, G., et al. (2011). Spatio-temporal transcriptome of the human brain. *Nature* **478**, 483–489.
- Katayama, K., Melendez, J., Baumann, J.M., Leslie, J.R., Chauhan, B.K., Nemkul, N., Lang, R.A., Kuan, C.Y., Zheng, Y., and Yoshida, Y. (2011). Loss of RhoA in neural progenitor cells causes the disruption of adherens junctions and hyperproliferation. *Proc. Natl. Acad. Sci. USA* **108**, 7607–7612.
- Kielar, M., Tuy, F.P., Bizzotto, S., Lebrand, C., de Juan Romero, C., Poirier, K., Oegema, R., Mancini, G.M., Bahi-Buisson, N., Olaso, R., et al. (2014). Mutations in Em1 lead to ectopic progenitors and neuronal heterotopia in mouse and human. *Nat. Neurosci.* **17**, 923–933.
- Lancaster, M.A., and Knoblich, J.A. (2014). Generation of cerebral organoids from human pluripotent stem cells. *Nat. Protoc.* **9**, 2329–2340.
- Lek, M., Karczewski, K.J., Minikel, E.V., Samocha, K.E., Banks, E., Fennell, T., O'Donnell-Luria, A.H., Ware, J.S., Hill, A.J., Cummings, B.B., et al.; Exome Aggregation Consortium (2016). Analysis of protein-coding genetic variation in 60,706 humans. *Nature* **536**, 285–291.
- Letunic, I., and Bork, P. (2011). Interactive Tree Of Life v2: online annotation and display of phylogenetic trees made easy. *Nucleic Acids Res.* **39**, W475–W478.
- Lewitus, E., Kelava, I., Kalinka, A.T., Tomancak, P., and Huttner, W.B. (2014). An adaptive threshold in mammalian neocortical evolution. *PLoS Biol.* **12**, e1002000.
- Li, H., and Durbin, R. (2009). Fast and accurate short read alignment with Burrows-Wheeler transform. *Bioinformatics* **25**, 1754–1760.
- Lui, J.H., Hansen, D.V., and Kriegstein, A.R. (2011). Development and evolution of the human neocortex. *Cell* **146**, 18–36.
- Malatesta, P., Hartfuss, E., and Götz, M. (2000). Isolation of radial glial cells by fluorescent-activated cell sorting reveals a neuronal lineage. *Development* **127**, 5253–5263.
- McKenna, A., Hanna, M., Banks, E., Sivachenko, A., Cibulskis, K., Kernysky, A., Garimella, K., Altshuler, D., Gabriel, S., Daly, M., and DePristo, M.A. (2010). The Genome Analysis Toolkit: a MapReduce framework for analyzing next-generation DNA sequencing data. *Genome Res.* **20**, 1297–1303.
- Narayanan, R., Pham, L., Kerimoglu, C., Watanabe, T., Castro Hernandez, R., Sokpor, G., Ulmke, P.A., Kiszka, K.A., Tonchev, A.B., Rosenbusch, J., et al. (2018). Chromatin remodeling BAF155 subunit regulates the genesis of basal progenitors in developing cortex. *iScience* **4**, 109–126.
- Noctor, S.C., Flint, A.C., Weissman, T.A., Dammerman, R.S., and Kriegstein, A.R. (2001). Neurons derived from radial glial cells establish radial units in neocortex. *Nature* **409**, 714–720.
- Noctor, S.C., Martínez-Cerdeño, V., Ivic, L., and Kriegstein, A.R. (2004). Cortical neurons arise in symmetric and asymmetric division zones and migrate through specific phases. *Nat. Neurosci.* **7**, 136–144.
- Nowakowski, T.J., Bhaduri, A., Pollen, A.A., Alvarado, B., Mostajo-Radji, M.A., Di Lullo, E., Haeussler, M., Sandoval-Espinosa, C., Liu, S.J., Velmeshev, D., et al. (2017). Spatiotemporal gene expression trajectories reveal developmental hierarchies of the human cortex. *Science* **358**, 1318–1323.
- Ostrem, B.E., Lui, J.H., Gertz, C.C., and Kriegstein, A.R. (2014). Control of outer radial glial stem cell mitosis in the human brain. *Cell Rep.* **8**, 656–664.
- Petrovski, S., Wang, Q., Heinzen, E.L., Allen, A.S., and Goldstein, D.B. (2013). Genic intolerance to functional variation and the interpretation of personal genomes. *PLoS Genet.* **9**, e1003709.
- Picco, N., García-Moreno, F., Maini, P.K., Woolley, T.E., and Molnár, Z. (2018). Mathematical modeling of cortical neurogenesis reveals that the founder population does not necessarily scale with neurogenic output. *Cereb. Cortex* **28**, 2540–2550.
- Pollen, A.A., Nowakowski, T.J., Chen, J., Retallack, H., Sandoval-Espinosa, C., Nicholas, C.R., Shuga, J., Liu, S.J., Oldham, M.C., Diaz, A., et al. (2015). Molecular identity of human outer radial glia during cortical development. *Cell* **163**, 55–67.
- Pruitt, K.D., Harrow, J., Harte, R.A., Wallin, C., Diekhans, M., Maglott, D.R., Searle, S., Farrell, C.M., Loveland, J.E., Ruef, B.J., et al. (2009). The consensus coding sequence (CCDS) project: identifying a common protein-coding gene set for the human and mouse genomes. *Genome Res.* **19**, 1316–1323.
- Rakic, P. (1988). Specification of cerebral cortical areas. *Science* **241**, 170–176.
- Reillo, I., de Juan Romero, C., García-Cabezas, M.A., and Borrell, V. (2011). A role for intermediate radial glia in the tangential expansion of the mammalian cerebral cortex. *Cereb. Cortex* **21**, 1674–1694.
- Rosenbloom, K.R., Sloan, C.A., Malladi, V.S., Dreszer, T.R., Learned, K., Kirkup, V.M., Wong, M.C., Maddren, M., Fang, R., Heitner, S.G., et al. (2013). ENCODE data in the UCSC Genome Browser: year 5 update. *Nucleic Acids Res.* **41**, D56–D63.

- Rosenbloom, K.R., Armstrong, J., Barber, G.P., Casper, J., Clawson, H., Diekhans, M., Dreszer, T.R., Fujita, P.A., Guruvadoo, L., Haeussler, M., et al. (2015). The UCSC Genome Browser database: 2015 update. *Nucleic Acids Res.* 43, D670–D681.
- Saito, T. (2006). In vivo electroporation in the embryonic mouse central nervous system. *Nat. Protoc.* 1, 1552–1558.
- Samocha, K.E., Robinson, E.B., Sanders, S.J., Stevens, C., Sabo, A., McGrath, L.M., Kosmicki, J.A., Rehnström, K., Mallick, S., Kirby, A., et al. (2014). A framework for the interpretation of de novo mutation in human disease. *Nat. Genet.* 46, 944–950.
- Sheen, V.L., Dixon, P.H., Fox, J.W., Hong, S.E., Kinton, L., Sisodiya, S.M., Duncan, J.S., Dubeau, F., Scheffer, I.E., Schachter, S.C., et al. (2001). Mutations in the X-linked filamin 1 gene cause periventricular nodular heterotopia in males as well as in females. *Hum. Mol. Genet.* 10, 1775–1783.
- Sherry, S.T., Ward, M.H., Kholodov, M., Baker, J., Phan, L., Smigielski, E.M., and Sirotkin, K. (2001). dbSNP: the NCBI database of genetic variation. *Nucleic Acids Res.* 29, 308–311.
- Smart, I.H., Dehay, C., Giroud, P., Berland, M., and Kennedy, H. (2002). Unique morphological features of the proliferative zones and postmitotic compartments of the neural epithelium giving rise to striate and extrastriate cortex in the monkey. *Cereb. Cortex* 12, 37–53.
- Sun, T., and Hevner, R.F. (2014). Growth and folding of the mammalian cerebral cortex: from molecules to malformations. *Nat. Rev. Neurosci.* 15, 217–232.
- Tavano, S., Taverna, E., Kalebic, N., Haffner, C., Namba, T., Dahl, A., Wilsch-Brauninger, M., Paridaen, J., and Huttner, W.B. (2018). Insm1 induces neural progenitor delamination in developing neocortex via downregulation of the adherens junction belt-specific protein Plekha7. *Neuron* 97, 1299–1314.e8.
- Van Der Auwera, G.A., Carneiro, M.O., Hartl, C., Poplin, R., Del Angel, G., Levy-Moonshine, A., Jordan, T., Shakir, K., Roazen, D., Thibault, J., et al. (2013). From FastQ data to high confidence variant calls: the Genome Analysis Toolkit best practices pipeline. *Curr. Protoc. Bioinformatics* 43, 11.10.1–11.10.33.
- Vermunt, M.W., Tan, S.C., Castelijn, B., Geeven, G., Reinink, P., de Bruijn, E., Kondova, I., Persengiev, S., Bontrop, R., Cuppen, E., et al.; Netherlands Brain Bank (2016). Epigenomic annotation of gene regulatory alterations during evolution of the primate brain. *Nat. Neurosci.* 19, 494–503.
- Voineagu, I., Wang, X., Johnston, P., Lowe, J.K., Tian, Y., Horvath, S., Mill, J., Cantor, R.M., Blencowe, B.J., and Geschwind, D.H. (2011). Transcriptomic analysis of autistic brain reveals convergent molecular pathology. *Nature* 474, 380–384.
- Watanabe, T., Hosoya, H., and Yonemura, S. (2007). Regulation of myosin II dynamics by phosphorylation and dephosphorylation of its light chain in epithelial cells. *Mol. Biol. Cell* 18, 605–616.
- Wu, D., Asiedu, M., Adelstein, R.S., and Wei, Q. (2006). A novel guanine nucleotide exchange factor MyoGEF is required for cytokinesis. *Cell Cycle* 5, 1234–1239.

## STAR★METHODS

### KEY RESOURCES TABLE

| REAGENT or RESOURCE                                  | SOURCE                    | IDENTIFIER                       |
|--|---------------------------|----------------------------------|
| <b>Antibodies</b>                                    |                           |                                  |
| Rabbit polyclonal anti-SOX2                          | Cell Signaling Technology | Cat# 2748SS; RRID: AB_823640     |
| Mouse monoclonal anti-MAP2                           | Sigma Aldrich             | Cat# M4403; RRID: AB_477193      |
| Mouse monoclonal anti-NeuN                           | Millipore                 | Cat# MAB377; RRID: AB_2298772    |
| Mouse monoclonal $\beta$ -catenin                    | Proteintech               | Cat# 610154; RRID: AB_397555     |
| Mouse monoclonal anti-PCNA                           | DAKO                      | Cat# M0879; RRID: AB_2160651     |
| Rabbit polyclonal anti-PALS1                         | Sigma Aldrich             | Cat# 07-708; RRID: AB_441951     |
| Phalloidin (Alexa Fluor 488-conjugated PHALLOIDIN)   | Thermo Fisher             | Cat# A12381; RRID: AB_2315147    |
| Chick polyclonal anti-GFP                            | Aves Lab                  | Cat# GFP-1020; RRID: AB_10000240 |
| Rabbit polyclonal anti-Pax6                          | Millipore                 | Cat# AB2237; RRID: AB_1587367    |
| Rabbit polyclonal anti-Tbr2                          | Millipore                 | Cat# AB2283; RRID: AB_10806889   |
| Rabbit polyclonal anti-Tbr1                          | Abcam                     | Cat# ab31940; RRID: AB_2200219   |
| Rabbit polyclonal anti-pH3                           | Millipore                 | Cat# 06-570; RRID: AB_310177     |
| Rabbit polyclonal anti-laminin                       | Abcam                     | Cat# ab11575; RRID: AB_298179    |
| Rabbit (clonality unknown) anti-MYPT1-pT853          | Cell Signaling Technology | Cat# 4563; RRID: AB_1031185      |
| Rabbit polyclonal anti-MYPT1                         | Cell Signaling Technology | Cat# 2634; RRID: AB_915965       |
| Mouse monoclonal anti-Ac-tubulin                     | Sigma Aldrich             | Cat# T6793; RRID: AB_477585      |
| Rabbit monoclonal anti-active caspase 3              | Abcam                     | Cat# ab32042; RRID: AB_725947    |
| Rabbit polyclonal anti-GAPDH                         | Sigma Aldrich             | Cat# G9545; RRID: AB_796208      |
| Mouse monoclonal anti-V5                             | Thermo Fisher Scientific  | Cat# R96025; RRID: AB_2556564    |
| Rabbit polyclonal anti-PLEKHG6_1                     | This paper                | N/A                              |
| Rabbit polyclonal anti-PLEKHG6_4                     | This paper                | N/A                              |
| <b>Chemicals, Peptides, and Recombinant Proteins</b> |                           |                                  |
| DMEM, GlutaMAX supplement                            | Thermo Fisher Scientific  | Cat# 61965026                    |
| Complete Protease Inhibitor                          | Roche                     | Cat# 11697498001                 |
| HyClone Fetal Bovine Serum                           | GE Healthcare             | Cat# SV30160.03HI                |
| DMEM:F12   | Thermo Fisher Scientific  | Cat# 11320033                    |
| Pluriton Reprogramming Medium                        | Stemgent                  | Cat# 00-0070                     |
| Carrier-free B18R Recombinant Protein                | Stemgent                  | Cat# 03-0017                     |
| Lipofectamin RNAiMAX Transfection Reagent            | Thermo Fisher Scientific  | Cat# 31985062                    |
| Lipofectamin 2000 Transfection Reagent               | Thermo Fisher Scientific  | Cat# 11668027                    |
| STEMPRO hESC SFM                                     | Thermo Fisher Scientific  | Cat# A1000701                    |
| Collagenase Type IV                                  | Thermo Fisher Scientific  | Cat# 17104019                    |
| StemPro Accutase Cell Dissociation Reagent           | Life Technologies         | Cat#A1110501                     |
| mTeSR1   | StemCell Technologies     | Cat# 05850                       |
| LDEV-Free Geltrex                                    | Thermo Fisher Scientific  | Cat# A1413302                    |
| Geltrex  | Thermo Fisher Scientific  | Cat# A1413302                    |
| Matrigel   | Corning                   | Cat# 354234                      |
| Rock inhibitor Y-27632(2HCL)                         | StemCell Technologies     | Cat# 72304                       |
| <b>Critical Commercial Assays</b>                    |                           |                                  |
| RNeasy mini kit                                      | QIAGEN                    | Cat# 74106                       |
| Maxima First Strand cDNA Synthesis Kit               | Thermo Fisher Scientific  | Cat# K1641                       |
| Fast SYBR Green Master Mix                           | Life Technologies         | Cat# 4385612                     |
| Wizard Genome DNA Purification Kit                   | Promega                   | Cat# A1620                       |

(Continued on next page)

**Continued**

| REAGENT or RESOURCE  | SOURCE   | IDENTIFIER  |
|--|--|---|
| Experimental Models: Cell Lines                                    |  |   |
| Human embryonic kidney 293T  | ATCC   | Cat# CRL-3216; RRID: CVCL_0063  |
| Mouse embryo teratocarcinoma P19                                   | ATCC   | Cat# CRL-1825; RRID: CVCL_2153  |
| Human induced pluripotent stem cells (hiPSCs)                      | ATCC   | Cat# CRL-2522, RRID: CVCL_3653  |
| NuFF3-RQ IRR Human newborn foreskin feeder fibroblast              | GlobalStem   | GSC-3404  |
| Experimental Models: Organisms/Strains                             |  |   |
| Mouse: C57BL/6J  | Jackson Laboratory   | Cat# 000664; RRID: SCR_004633;<br><a href="https://www.jax.org/">https://www.jax.org/</a>     |
| Oligonucleotides   |  |   |
| miRNA targeting sequence: Plekhg6 #1: CTAACCAGCAATC TGTCACCT       | This paper   | N/A   |
| miRNA targeting sequence: Plekhg6 #2: TGCACCTGAACTA ACCAGCAA       | This paper   | N/A   |
| miRNA targeting sequence: Plekhg6 #3: TACTGTGGAAATC TGGGTCGT       | This paper   | N/A   |
| miRNA targeting sequence: PLEKHG6_4: CCACAGGCAAAT GAAGGAATG        | This paper   | N/A   |
| Recombinant DNA  |  |   |
| Expression plasmid: pCAGGS   | (Cappello et al., 2013)  | N/A   |
| Expression plasmid: pcDNA6.2-GW/miR                                | Invitrogen   | Cat# K493600  |
| Expression plasmid: RhoA*GFP (fast-cycling)                        | C. Brakebush gift (Cappello et al., 2012)                                  | N/A   |
| Expression plasmid: p3xFLAG-CMV/PLEKHG6_4                          | This paper   | N/A   |
| Expression plasmid: p3xFLAG-CMV/PLEKHG6_1                          | This paper   | N/A   |
| Expression plasmid: p3xFLAG-CMV/PLEKHG6_744                        | This paper   | N/A   |
| Expression plasmid: pcDNA3.1V5/His-PLEKHG6_4                       | This paper   | N/A   |
| Software and Algorithms  |  |   |
| Burrows-Wheeler Aligner  | (Li and Durbin, 2009)  | <a href="http://bio-bwa.sourceforge.net/">http://bio-bwa.sourceforge.net/</a>                 |
| Genome Analysis Toolkit (GATK)                                     | (DePristo et al., 2011; McKenna et al., 2010; Van Der Auwera et al., 2013) | <a href="https://www.broadinstitute.org/gatk/">https://www.broadinstitute.org/gatk/</a>       |
| Picard Tools   | Broad Institute  | <a href="http://broadinstitute.github.io/picard/">http://broadinstitute.github.io/picard/</a> |
| Other  |  |   |
| Exome Aggregation Consortium (ExAC), Cambridge, MA,                | N/A  | <a href="http://exac.broadinstitute.org">http://exac.broadinstitute.org</a>                   |
| Online Mendelian Inheritance in Man (OMIM)                         | N/A  | <a href="http://www.omim.org/">http://www.omim.org/</a>                                       |
| Allen Brain Atlas BrainSpan project                                | N/A  | <a href="http://www.brainspan.org/">http://www.brainspan.org/</a>                             |
| Encode Project   | N/A  | <a href="https://www.encodeproject.org/">https://www.encodeproject.org/</a>                   |
| UCSC Genome Browser  | N/A  | <a href="https://genome.ucsc.edu/">https://genome.ucsc.edu/</a>                               |
| 1000 Genomes   | N/A  | <a href="http://www.internationalgenome.org/">http://www.internationalgenome.org/</a>         |
| Ensembl Genome Browser   | N/A  | <a href="http://www.ensembl.org/index.html">http://www.ensembl.org/index.html</a>             |
| NHLBI Exome Sequencing Project (ESP) Exome Variant Server, ESP6500 | N/A  | <a href="http://evs.gs.washington.edu/EVS/">http://evs.gs.washington.edu/EVS/</a>             |
| GenBank  | N/A  | <a href="https://www.ncbi.nlm.gov/genbank/">https://www.ncbi.nlm.gov/genbank/</a>             |

**CONTACT FOR REAGENT AND RESOURCE SHARING**

Further information and requests for resources and reagents should be directed to and will be fulfilled by the Lead Contact, Silvia Cappello ([silvia\\_cappello@psych.mpg.de](mailto:silvia_cappello@psych.mpg.de)).



## EXPERIMENTAL MODEL AND SUBJECT DETAILS

### PH Trios

We utilized 65 trios (affected child and both parents) characterized and contributed by us in a previous study (Heinzen et al., 2018). Study participants can be identified here through the prefix 'pvhnz' in the cohort identifier table, where data describing the sex of these participants can also be identified. All study participants were ascertained by physician referral, presumed sporadic disease based on patient and family interview, and consented to participate under the University of Otago consent protocol. Ethical approval was obtained from the Southern regional Ethics Committee O03/016 and the New Zealand Ethics Committee MEC08/08/094. Specifically this ethical approval does not allow for the general sharing of individual exome sequences on confidentiality grounds.

### iPSC generation and human organoids

Male human iPSCs were reprogrammed from human newborn foreskin fibroblasts (CRL-2522, ATCC). iPSCs were authenticated after reprogramming by karyotyping. The use of iPSCs to generate cerebral organoids was approved by the Ethics Commission of LMU (Ludwig-Maximilians-Universität München), with the association number 115-16. iPSCs and human organoids were cultured at 37°C, 5% CO<sub>2</sub> and ambient oxygen level on Geltrex coated plates in mTeSR1 medium with daily medium change. Electroporations were performed in cerebral organoids at 42 days stages after the initial plating of the cells and fixed 4 or 7 days post electroporation.

### Mice

All the animals used in this work were kept in the animal facility of the Helmholtz Zentrum München. All the experimental procedures were performed in accordance with German and European Union guidelines. Animals were maintained on a 12 hour light-dark cycle. The day of vaginal plug was considered as embryonic day 0 (E0). In this study the C57BL/6J mouse line was used. All animals used for in utero electroporation were female between 4 – 6 months of age.

## METHOD DETAILS

### Whole-exome sequencing

Whole-exome sequencing was carried out by Otogenetics Corporation (Norcross, GA, USA). Sequencing libraries were prepared from genomic DNA extracted from leukocytes of parents and patients using Wizard® Genomic DNA Purification Kit (Promega, Cat. A1620) following the manufacturer's instructions. Library DNA was exome enriched using the Agilent SureSelect Human All Exon V4+UTRs capture kit, and sequenced on an Illumina HiSeq2000, Illumina, San Diego, CA using 100 bp paired-end reads. Alignment of the sequenced DNA fragments to the Ensembl Genome Browser human genome assembly (GRCh37) was carried out using the Burrows-Wheeler Aligner (MEM algorithm) v.0.7.12. After alignments were produced for each individual separately, the data was locally realigned around indels followed by base quality score recalibration using Genome Analysis Tool Kit (GATK) Best Practices IndelRealigner (version 3.4-46; Broad Institute). Duplicate reads were removed using PICARD (version 1.140; Broad Institute). Individual variant calling was undertaken using the GATK HaplotypeCaller, followed by multisample genotyping and variant quality score recalibration. Variant call format file (VCF) gene context annotation was added using SnpEff v.4.1L. Allele frequencies were obtained from 1000 Genomes Project phase 1, NHLBI GO Exome Sequencing Project ESP6500 and the Exome Aggregation Consortium (ExAC) via the GATK VariantAnnotator.

### Whole-exome sequencing variant calling

All alignments with loci bearing putative *de novo* mutations were extracted from the multisample VCF using GATK SelectVariants and SnpSift v.4.1L (SnpEff) that met the following criteria: (1) the read depth should be  $\geq 8$  within the patient; (2) at least 20% of the reads should carry the alternate allele; (3)  $< 5\%$  of the reads in either parent should carry the alternative allele; (4) at least two alleles must be observed in the proband; (5) the genotype quality (GQ) score for the offspring's alternate allele should be 99; (6) the normalized, phred-scaled genotype likelihood (PL) scores in both parents for the three possible genotypes 0/0, 0/1 and 1/1, where 0 is the reference allele and 1 is the alternative allele, should be  $> 0$ ,  $> 20$  and  $> 20$ , respectively. Candidate *de novo* mutations were also absent from population controls, including a set of 107 internally sequenced controls and the 60,706 individuals whose single nucleotide variant data are reported in ExAC. All candidate *de novo* mutations were Sanger sequenced using the relevant proband and parents for confirmation. Using our filtering approach across the entire cohort of 65 individuals we identified 177 potential *de novo* mutations, of which, 50 were independently validated by Sanger sequencing (28% validation rate). Of the 127 variants that did not validate, 21 were false negatives in parents while 106 were false positives in the probands, implying this analysis overall had high sensitivity to detect *de novo* variants at the cost of lower specificity.

Loci bearing putative recessive variants were extracted from the VCF that met the following criteria: (1) the read depth should be  $\geq 8$  or 20 for compound heterozygous or homozygous recessive genotype calls in the patient, respectively; (2) at least 20% and 90% of the reads in the patient should carry the alternate allele for candidate compound heterozygous and homozygous genotypes, respectively; (3) in the parents, at least one individual requires a read depth  $\geq 30$ ; (4) candidate recessive variants should not be present in

population controls, including a set of 107 internally sequenced controls and the 60,706 individuals whose single nucleotide variant data are reported in ExAC. All candidate recessive variants were Sanger sequenced using the relevant proband and parents for confirmation.

## Burden analysis

### Modeling apical and basal progenitor gene mutation rates

To assess whether there is an excess of *de novo* variants identified specifically within gene sets that define apical and basal radial glia (aRG and bRG, respectively) we used loci that define these functional classes for each cell type as outlined by others (Pollen et al., 2015). The expected rate for each gene set was calculated by establishing the gene-specific mutation rates [presented as  $\log_{10}(\text{prob})$ ] provided in (Samocha et al., 2014). These gene-specific mutation rates are based primarily on estimated triplet-specific mutations rates, thus taking into account sequence context and gene size, by way of validation, they accurately predict the amount of synonymous variation seen in coding sequences. Thus, for genes defining a bRG transcriptomic signature the expected number of *de novo* variants was 0.26 for a denominator of 67 genes (defined in (Pollen et al., 2015)) in a cohort of 65 patients using the approach devised by (Samocha et al., 2014). Similarly, for the aRG transcriptomic signature the expected number of *de novo* variants was 0.13 for a denominator of 33 genes (defined in (Pollen et al., 2015)) in a cohort of 65 patients using the approach of (Samocha et al., 2014).

### Assessing for gene set enrichment

For determining overlap with *de novo* mutations, functional gene classes were defined as follows. ‘FMRP’ are genes encoding transcripts that bind to FMRP (Darnell et al., 2011). ‘Chromatin’ indicates chromatin modifiers as defined by GO (<http://www.geneontology.org/>). ‘PSD’ is a set of genes encoding proteins that have been identified in postsynaptic densities (Bayés et al., 2011). ‘Mendelian’ represent positionally identified human disease genes (Feldman et al., 2008), and ‘Essential’ genes are human orthologs of mouse genes associated with lethality in the Mouse Genome Database (Blake et al., 2011). ‘Embryonic’ genes are those expressed in post-mortem human embryonic brains (Voineagu et al., 2011), derived from downloaded expression data (Kang et al., 2011). All gene lists have also been used elsewhere (Iossifov et al., 2014). Tests assessing excess were carried out using the Exact binomial test (two-tailed) with the expected rate for each gene set being calculated using the approach described above and of (Samocha et al., 2014).

### Analysis of PLEKHG6 evolutionary conservation

Ensembl, NCBI and USCS genome bioinformatics data were assessed for the first exon coding sequence orthologs of PLEKHG6 isoform 1 and 4 across species. The evolutionary tree was generated using iTOL (Letunic and Bork, 2011).

### Reprogramming of human fibroblasts to induced pluripotent stem cells (iPSCs)

Male human iPSCs were reprogrammed from human newborn foreskin fibroblasts (CRL-2522, ATCC).  $2.5 \times 10^5$  NuFF3-RQ IRR human newborn foreskin feeder fibroblasts (GSC-3404, GlobalStem) were seeded per well of a 6-well tissue culture dish with advanced MEM (12491015, Thermo Fisher Scientific) supplemented with 5% HyClone Fetal Bovine Serum (SV30160.03HI, GE Healthcare), 1% MEM NEAA and GlutaMAX (11140050; 35050061 Thermo Fisher Scientific). On day 1, 70%–80% confluent CRL-2522 fibroblasts were dissociated using 0.25% Trypsin-EDTA (25200056, Life Technologies), counted and seeded on the NuFF3-RQ cells at two different densities:  $2 \times 10^4$  cells/well and  $4 \times 10^4$  cells/well. On day 2, the medium was changed to Pluriton Reprogramming Medium (00-0070, Stemgent) supplemented with 500 ng/ml carrier-free B18R Recombinant Protein (03-0017, Stemgent). On days 3–18, a cocktail of modified mRNAs (mmRNAs) containing OCT4, SOX2, LIN28, C-MYC, and KLF mmRNAs at a 3:1:1:1:1 stoichiometric ratio was transfected daily. For that purpose, the mmRNAs were mixed in a total volume of 105  $\mu$ l and were combined with a mix of 92  $\mu$ l Opti-MEM I Reduced Serum Medium and 13  $\mu$ l Lipofectamine RNAiMAX Transfection Reagent (31985062, Thermo Fisher Scientific) after separate incubation at RT for 15 min. Cells were transfected for 4hrs, washed and fresh reprogramming medium supplemented with B18R was added to the cultures. The mmRNAs with the following modifications: 5-Methyl CTP, a 150 nt poly-A tail, ARCA cap and Pseudo-UTP were obtained from the RNA CORE unit of the Houston Methodist Hospital. 5 days after the first transfection, the first morphological changes were noticed, while the first induced pluripotent stem cell (iPSC) colonies appeared by day 12–15. On day 16, the medium was changed to STEMPro hESC SFM (A1000701, Thermo Fisher Scientific) for five days. Harvesting of the iPSC colonies was performed after 40min incubation at 37°C with 2mg/ml Collagenase Type IV (17104019, Thermo Fisher Scientific) solution in DMEM/F12 (31331093, Thermo Fisher Scientific). The iPSCs were plated on  $\gamma$ -irradiated mouse embryonic fibroblasts (MEFs) and grown in STEMPro hESC SFM for 10 additional passages. After that the iPSCs were further cultured in a feeder-free culture system, using mTeSR1 (05850, StemCell Technologies) on plates coated with LDEV-Free Geltrex (A1413302, Thermo Fisher Scientific). iPSCs were authenticated after reprogramming by karyotyping.

### iPSC culture

iPSCs were cultured at 37°C, 5% CO<sub>2</sub> and ambient oxygen level on Geltrex coated plates in mTeSR1 medium with daily medium change. For passaging, iPSC colonies were incubated with StemPro Accutase Cell Dissociation Reagent (A1110501, Life Technologies) diluted 1:4 in PBS for 4 minutes. Pieces of colonies were washed off with DMEM/F12, centrifuged for 5 min. at 300 x g and resuspended in mTeSR1 supplemented with 10  $\mu$ M Rock inhibitor Y-27632(2HCl) (72304, StemCell Technologies) for the first day.

### Cerebral organoid generation

Cerebral organoids were generated as previously described (Lancaster and Knoblich, 2014). Briefly iPSCs were dissociated into single cells using StemPro Accutase Cell Dissociation Reagent (A1110501, Life Technologies) and plated in the concentration of 9000 single iPSCs/well into low attachment 96-well tissue culture plates in hES medium (DMEM/F12GlutaMAX supplemented with 20%

Knockout Serum Replacement, 3% ES grade FBS, 1% Non-essential amino acids, 0.1mM 2-mercaptoethanol, 4ng/ml bFGF and 50  $\mu$ M Rock inhibitor Y27632) for 6 days in order to form embryoid bodies (EBs). Rock inhibitor Y27632 and bFGF were removed on the 4<sup>th</sup> day. On day 6 EBs were transferred into low attachment 24-well plates in NIM medium (DMEM/F12GlutaMAX supplemented with 1:100 N2 supplement, 1% Non-essential amino acids and 5  $\mu$ g/ml Heparin) and cultured for additional 6 days. On day 12 EBs were embedded in Matrigel (Corning, 354234) drops and then they were transfer in 10cm tissue culture plates in NDM minus A medium (DMEM/F12GlutaMAX and Neurobasal in ratio 1:1 supplemented with 1:100 N2 supplement 1:100 B27 without Vitamin A, 0.5% Non-essential amino acids, insulin 2.5  $\mu$ g/ml, 1:100 Antibiotic-Antimycotic and 50 $\mu$ M 2-mercaptoethanol) in order to form organoids. 4 days after Matrigel embedding cerebral organoids were transfer into an orbital shaker and cultured until electroporation in NDM plus A medium (DMEM/F12GlutaMAX and Neurobasal in ratio 1:1 supplemented with 1:100 N2 supplement 1:100 B27 with Vitamin A, 0.5% Non-essential amino acids, insulin 2.5  $\mu$ g/ml, 1:100 Antibiotic-Antimycotic and 50  $\mu$ M 2-mercaptoethanol). During the whole period of cerebral organoid generation, cells were kept at 37°C, 5% CO<sub>2</sub> and ambient oxygen level with medium changes every other day. After transferring the cerebral organoids onto the shaker medium was changed twice per week.

#### **Assessing PLEKHG6\_4 knockdown efficiencies**

Efficiency of miRNA knockdown targeted by PLEKHG6\_4 (miPLEKHG6\_4) was determined by transient co-transfection with a PLEKHG6\_4 expression plasmid (pcDNA3.1V5/His-*PLEKHG6\_4*), and data expressed as relative PLEKHG6\_4 expression. Specifically, HEK293FT cells were transfected with miPLEKHG6\_4 (400ng and 800ng), and a mock transfected control followed by growth for 22 hours before secondary transfection with pcDNA3.1V5/His-*PLEKHG6\_4* (400ng). After a further 22 hours of growth total cell lysates were prepared and subjected to western blot analysis using anti-V5 antibody (mouse, Thermo Fisher Scientific Cat # R96025, 1:2500) to detect tagged PLEKHG6\_4 expression. Relative expression of PLEKHG6\_4 was calculated for each miPLEKHG6\_4 sample as the ratio of PLEKHG6\_4 expression to mock transfected control. Data presented as mean ( $\pm$ SEM). Mann-Whitney U test; \*  $p < 0.05$ .

#### **Electroporation of cerebral organoids**

Cerebral organoids were kept in antibiotics-free conditions prior to electroporation. Electroporations were performed in cerebral organoids at 42 days stages after the initial plating of the cells and fixed 4 or 7 days post electroporation. During the electroporation cerebral organoids were placed in an electroporation chamber (Harvard Apparatus, Holliston, MA, USA) under a stereoscope and using a glass microcapillary 1–2  $\mu$ L of plasmid DNAs at final concentration of 1  $\mu$ g/ $\mu$ L was injected together with Fast Green (0.1%, Sigma) into different ventricles of the organoids. Cerebral organoids were subsequently electroporated with 5 pulses applied at 80V for 50ms each at intervals of 500ms using the Electroporator ECM830 (Harvard Apparatus). Following electroporation cerebral organoids were kept for additional 24 hours in antibiotics-free media, and then changed into the normal media until fixation. Cerebral organoids were fixed using 4% PFA for 1h at 4°C, cryopreserved with 30% sucrose and then stored in –20°C. For immunofluorescence, 16  $\mu$ m cryosections were prepared. For each experiment, many independent ventricles per organoid from 4–6 different organoids per condition were analyzed. pCAGGS was used as the control plasmid. Human *PLEKHG6* isoform 4 targeting miRNA-expressing constructs [miPLEKHG6\_4 (5'- ccacaggcaaatgaaggaatg –3')] were cloned into the pcDNA6.2-GW/miR vector (Blockit, Invitrogen) according to the manufacturer's instructions. Plasmids were subsequently recombined into pCAGGS destination vector.

#### **Immunofluorescence of human cerebral organoid cells**

Tissues were processed as per mouse cortical tissue. Before sections were blocked they were boiled in calcium chloride (1% solution) for 5 minutes. Sections were blocked and permeabilized in 0.25% Triton X-100, 4% normal donkey serum in PBS. Sections were then incubated with primary antibodies in 0.1% Triton X-100, 4% normal donkey serum at the following dilutions: PCNA (mouse IgG2a, DAKO, Cat. # M0879, 1:40), MAP2 (mouse IgG1, Sigma, Cat. # M4403, 1:300), *PLEKHG6* isoform one and isoform four (rabbit, MIMOTOPES, 1:1000, each). Sections were incubated overnight at 4°C. The next day slides were washed in three times in PBS and then treated as per the manufacturer's instructions for the Thymid kit (ThermoFisher, Cat. # T20922) to amplify the detection of *PLEKHG6* isoforms one and four, separately. The appropriate secondary fluorophore antibodies were used for PCNA and MAP2 as per the manufacturer's instructions. *PLEKHG6* isoform one and four antibodies were generated, specifically, from MIMOTOPES (Clayton, Australia). The peptides used to establish immunogenicity were N-MKAFGPPHEGLQLGL-C and N-MGCRLHAPGEKAAH-C for isoform one and four, respectively. Both peptides were conjugated to KLH through Cys coupling at their C-termini. For all the other immunostainings which were performed in human cerebral organoids the following protocol was used. Sections were post-fixed with 4% PFA for 10 mins, permeabilized in 0.3% Triton X-100 and then blocked with 0.1% Tween, 3% BSA and 10% normal goat serum. Sections then incubated with primary antibodies diluted in blocking solution. GFP (chick, Aves Lab, Cat # GFP-1020, 1:1000), Sox2 (rabbit, Cell Signaling Cat # 2748S, 1:500),  $\beta$ -catenin (mouse, Proteintech Cat # 610154, 1:500), NeuN (mouse, Millipore Cat # MAB377, 1:500), Phalloidin (Alexa Fluor 488-conjugated PHALLOIDIN, Thermo Fisher Cat # A12379, 1:80), PALS1 (rabbit, Sigma Aldrich Cat # 07-708, 1:500).

#### **Anesthesia**

To perform in utero operations, mice were anaesthetised by subcutaneous injection of a solution containing: Fentanyl (0.05 mg/kg), Midazolam (5 mg/kg) and Medetomidine (0.5 mg/kg). The anesthesia was terminated with a subcutaneous injection of a solution composed of Buprenorphine (0.1 mg/kg), Atipamezol (1.5 mg/kg) and Flumazenil (0.5 mg/kg).

### ***In utero electroporation***

Surgery was performed on animals in accordance with the guidelines of Government of Upper Bavaria under license number 55.2-1-54-2532-79-2016. E13 pregnant dams were anesthetized and operated on as previously described (Saito, 2006). In brief, the shaved abdomen was opened by caesarean section in order to expose the uterine horns. These were kept wet and warm by continuous application of pre-warmed saline. Endotoxin free vectors – diluted to 1.5  $\mu\text{g}/\mu\text{L}$  – were mixed in Fast green (2.5  $\text{mg}/\mu\text{L}$ , Sigma). 1  $\mu\text{L}$  of mix was injected into the ventricle with the aid of glass capillaries (self-made with a micropipette puller). DNA was electroporated into the telencephalon with five pulses of 38 mV for 100 ms each. At the end of the entire electroporation procedure, the uterine horns were repositioned into the abdominal cavity, which was then filled with pre-warmed saline. The abdominal wall was closed by surgical sutures (Ethicon, Cat. # K832H). Anaesthesia is reversed as described above and animals were monitored appropriately. At E14 (one day post electroporation) or E16 (three days post electroporation) operated animals were sacrificed by cervical dislocation. Embryos were placed in HBSS (Hank's Balanced Salt Solution – GIBCO, Life Technologies) supplemented with 10 mM HEPES (GIBCO, Life Technologies). Embryos were dissected and brains fixed. pCAGGS was used as the control plasmid. *Plekhhg6* targeting miRNA-expressing constructs [miRNA1 (5'- ctaaccagcaatctgtcacct -3'), miRNA2 (5'- tgcacctgaactaaccagcaa -3'), miRNA3 (5'- tactgtggaatctgggtcgt -3')] were cloned into the pcDNA6.2-GW/miR vector (Blockit, Invitrogen) according to the manufacturer's instructions. Plasmids were subsequently recombined into pCAGGS destination vector.

### ***Immunofluorescence of mouse cortical tissue***

Mouse cortical tissues were fixed in 4% paraformaldehyde for 20 min at 4°C followed by washing in PBS three times 10 min. Tissues were allowed to sink in 30% sucrose overnight and then embedded into molds (Polysciences, Cat. # 18646A-1) using Tissue-Tek (Hartenstein, Cat. # TTEK) and frozen on dry ice. Tissue was then stored at -20°C until it was cryosectioned in 20  $\mu\text{m}$  sections with a Cryostat (Leica). Sections were blocked and permeabilized in 0.25% Triton X-100, 4% normal donkey serum in PBS. Sections were then incubated with primary antibodies in 0.1% Triton X-100, 4% normal donkey serum at the following dilutions: GFP (chick, Aves Lab, Cat. # GFP-1020, 1:500), Pax6 (rabbit, Merck-Millipore, Cat. # AB2237, 1:500), pHistone H3 mitosis MKR (pH3) (rabbit, Merck-Millipore, Cat. # 06-570, 1:1000), Tbr2 (rabbit, Merck-Millipore, Cat. # AB2283, 1:500), Tbr1 (rabbit, Abcam, Cat. # ab31940, 1:500), laminin (rabbit, Abcam, Cat. # ab11575, 1:500), ac-tubulin (mouse, Sigma, Cat # T6793, 1:800 and active caspase-3 (rabbit, Abcam, Cat. # ab32042, 1:500). Sections were incubated overnight at 4°C. The next day slides were washed three times in PBS and then treated as per the manufacturer's instructions with the appropriate secondary fluorophore antibodies.

### ***RhoGAP activity assay***

DNA constructs expressing full-length and truncated version of human *PLEKHG6* isoform 1 and 4 were generated by standard cloning techniques. Expression constructs were transiently transfected into HEK293 cells with Lipofectamine 2000 (Invitrogen, Cat. # 11668-019) according to the manufacturer's instructions. Cells were lysed 20 hours post transfection in 1x tris buffered saline (TBS), 1% (v/v) Triton X-100 and Complete Protease Inhibitor (Roche) on ice for 20 min. Cell debris was then pelleted through centrifugation at 13,000 rpm 4°C for 10 min. 20  $\mu\text{L}$  of protein lysate was combined with protein loading dye (final concentration: 50 mM Tris pH 6.8, 10% glycerol, 2% SDS, 6% 2-mercaptoethanol and 1% w/v Bromo blue) and denatured at 95°C for 5 min, before being subjected to SDS-PAGE. Immunoblot analysis was performed using anti-myosin phosphate target protein 1 (MYPT1; rabbit, Cell Signaling Technology, Cat. # 2634, 1:1000), anti-MYPT1-pT853 (rabbit, Cell Signaling Technology, Cat. # 4563, 1:1000) and anti-GAPDH (rabbit, Sigma-Aldrich, Cat. # G9545, 1:3000).

## **QUANTIFICATION AND STATISTICAL ANALYSIS**

Analyses were performed using the R statistical software in the case of the burden analyses, with all other tests analyzed in Graphpad Prism 7.0 software. To compare the statistical difference between two experimental groups we used an unpaired Mann-Whitney U test. For assessing the statistical difference between at least three experimental groups, One way-ANOVA was used. Fisher's exact test was used for assessing categorical data in Table 1, Figure 3 and Table S4. Data are represented as mean  $\pm$  s.e.m. In the case of categorical data, we did not correct p values for multiple comparisons because our primary hypotheses focused on *de novo* variants with all subsidiary tests not being part of the primary examination of the hypothesis. Experimental repeat numbers and statistical test performed for each dataset are described in the main text within each respective figure legend. For each experiment, embryos from at least two different females were used with the total number of cells counted shown below each treatment bar in each graph of the figure. Significance was set at  $p = 0.05$ . For *in utero* electroporations, all quantifications were made in at least 5 embryos. For electroporations performed in cerebral organoids, several independent ventricles were analyzed from 4-6 different organoids per condition from two independent batches.



## Supplemental Information

### **A Primate-Specific Isoform of *PLEKHG6***

#### **Regulates Neurogenesis and Neuronal Migration**

**Adam C. O'Neill, Christina Kyrousi, Johannes Klaus, Richard J. Leventer, Edwin P. Kirk, Andrew Fry, Daniela T. Pilz, Tim Morgan, Zandra A. Jenkins, Micha Drukker, Samuel F. Berkovic, Ingrid E. Scheffer, Renzo Guerrini, David M. Markie, Magdalena Götz, Silvia Cappello, and Stephen P. Robertson**

**Table S1: List of candidate *de novo* mutations identified in 65 PH trios analysed in this study. Related to Figure 1**

| Individual | Candidate gene(s) | Chr | Position  | Nucleotide    | Protein         |
|------------|-------------------|-----|-----------|---------------|-----------------|
| 769        | <i>CALM3</i>      | 19  | 47111760  | c.200C>T      | p.Pro67Leu      |
| 780        | <i>PIK3R1</i>     | 5   | 67522777  | c.274C>T      | p.Pro92Ser      |
| 1226       | <i>CLEC16A</i>    | 16  | 11136118  | c.1668G>C     | p.K556N         |
| 1291       | <i>GOLGB1</i>     | 3   | 121414605 | c.4765CCTTdel | p.Glu1589fs*    |
| 1337       | <i>C17orf104</i>  | 17  | 42744834  | c.1555C>G     | p.Gln519Glu     |
| 1490       | <i>SCAF8</i>      | 6   | 155124724 | c.830A>C      | p.Glu277Ala     |
| 1492       | <i>GATAD2A</i>    | 19  | 19576161  | c.7G>A        | p.Glu3Lys       |
|            | <i>GOLGA4</i>     | 3   | 37330777  | c.643A>G      | p.Arg215Gly     |
|            | <i>EFCAB1</i>     | 8   | 49637324  | c.614G>A      | p.Pro205Ser     |
| 1493       | <i>RYR2</i>       | 1   | 237881777 | c.10510G>A    | p.Glu3504Lys    |
| 2317       | <i>CNTROB</i>     | 17  | 7849070   | c.1759C>T     | p.Pro587Ser     |
| 2506       | <i>JAKMIP3</i>    | 10  | 133967302 | c.2107C>T     | p.Arg703Trp     |
| 2808       | <i>CNTN2</i>      | 1   | 205027694 | IVS4+2A>G     | Splice defect   |
|            | <i>TNMD</i>       | X   | 99854069  | c.642insA     | p.G215Rfs*3     |
|            | <i>ACIN1</i>      | 14  | 23549258  | c.1286A>G     | p.K429R         |
| 3037       | <i>LMX1A</i>      | 1   | 165324772 | c.24_25insA   | p.Glu9Argfs*49  |
| 3040       | <i>LRRK2</i>      | 12  | 40631906  | IVS5-1G>T     | Splice defect   |
|            | <i>KLHL10</i>     | 17  | 40004255  | c.1523C>T     | p.Arg508His     |
|            | <i>KIFAP3</i>     | 1   | 170003611 | c.644C>G      | p.Thr215Ser     |
| 3051       | <i>ARHGEF10</i>   | 8   | 1900958   | c.3485C>T     | p.Pro1162Leu    |
| 3054       | <i>GFRA1</i>      | 10  | 117853290 | c.923C>G      | p.Cys308Ser     |
| 3107       | <i>ATAD3C</i>     | 1   | 1389837   | c.335C>T      | p.Thr112Met     |
| 3160       | <i>LRIG3</i>      | 12  | 59280626  | c.958C>T      | p.Gly320Ser     |
| 3171       | <i>SPRY2</i>      | 13  | 80911693  | c.148G>A      | p.Arg50*        |
| 3176       | <i>FAM46D</i>     | X   | 79699198  | c.1160G>A     | p.Gly387Asp     |
| 3183       | <i>GLUL</i>       | 1   | 182357871 | c.1A>C        | p.Met1Arg       |
| 3242       | <i>LGALS3BP</i>   | 17  | 76968308  | c.1108G>A     | p.Glu370Lys     |
| 3288       | <i>CDK13</i>      | 7   | 40085606  | c.2525A>G     | p.Asn842Ser     |
| 3296       | <i>SAMD11</i>     | 1   | 878375    | c.1501C>T     | p.Leu501Phe     |
| 3338       | <i>OSBPL1A</i>    | 18  | 21921567  | c.338G>C      | p.Ser113Thr     |
|            | <i>PTPRJ</i>      | 11  | 48145255  | c.708*>+C     | p.Cys236Cysfs*5 |
| 3341       | <i>GPR98</i>      | 5   | 90079771  | c.13550T>C    | p.Ile4517Thr    |
|            | <i>NOL10</i>      | 2   | 10811767  | c.299G>T      | p.Gly100Val     |

**Table S1: continued**

| Individual | Candidate gene(s) | Chr | Position  | Nucleotide       | Protein       |
|------------|-------------------|-----|-----------|------------------|---------------|
| 3344       | <i>PRPF6</i>      | 20  | 62612665  | c.67C>T          | p.Arg23Trp    |
| 3350       | <i>ZNF790</i>     | 19  | 37310002  | c.1244T>C        | p.Ile415Thr   |
| 3390       | <i>ZNF12</i>      | 7   | 6731756   | c.817G>C         | p.Glu273Gln   |
| 3412       | <i>HNRNPA0</i>    | 5   | 137089208 | c.548G>T         | p.Gly183Val   |
| 3433       | <i>DPP9</i>       | 19  | 4703897   | IVS5-C>T         | Splice defect |
| 3480       | <i>PTPRD</i> *    | 9   | 8528586   | c.546G>C         | p.Arg182Ser   |
|            | <i>MYH2</i>       | 17  | 10440684  | c.1763T>G        | p.Val588Gly   |
| 3483       | <i>PI4KA</i>      | 22  | 21073066  | c.5161G>A        | p.Gly1721Ser  |
| 3486       | <i>NEB</i>        | 2   | 152521300 | c.5314_5315delTC | p.Ser1772fs   |
|            | <i>MEX3B</i>      | 15  | 82336718  | c.493G>A         | p.Val165Met   |
| 3489       | <i>SUSD2</i>      | 22  | 24581633  | c.1075C>T        | p.Arg359Trp   |
| 3492       | <i>RAB11FIP5</i>  | 2   | 73303277  | c.1602delT       | p.Pro534fs    |
| 3498       | <i>TTN</i>        | 2   | 179449471 | c.64897C>T       | p.Arg21633Trp |
| 3504       | <i>ZNF117</i>     | 7   | 64438651  | c.1298T>C        | p.Ile433Thr   |
|            | <i>ABAT</i> *     | 16  | 8875151   | c.1426T>G        | p.Ser476Ala   |
|            | <i>ZC3H4</i>      | 19  | 47570329  | c.3196G>A        | p.Asp1066Asn  |
|            | <i>DCBLD2</i>     | 3   | 98538048  | c.1085C>A        | p.Thr362Lys   |

\* Transcript ENST00000537002 only. ‡ Transcript ENST00000569156 only. Both transcripts are also only present within *Homo sapiens*.

**Table S2: List of candidate biallelic mutations identified in 65 PH trios analysed in this study. Related to Figure 1**

| Individual | Candidate gene(s) | Chr | Position  | Nucleotide            | Protein            |
|------------|-------------------|-----|-----------|-----------------------|--------------------|
| 533        | <i>F5</i>         | 1   | 169509859 | c.4449T>G             | p.Met1490Arg       |
|            | <i>F5</i>         | 1   | 169515818 | c.1624A>G             | p.Ile542Val        |
| 1203       | <i>MOB2</i>       | 11  | 1502019   | c.207delC             | p.Phe69Phefs*127   |
|            | <i>MOB2</i>       | 11  | 1491530   | c.679C>T              | p.Glu227Lys        |
| 1291       | <i>SVEP1</i>      | 9   | 113208279 | c.4301C>T             | p.Gly1434Asp       |
|            | <i>SVEP1</i>      | 9   | 113192266 | c.5549G>A             | p.Pro1850Leu       |
| 1493       | <i>COL5A1</i>     | 2   | 189929302 | c.1697G>A             | p.Pro566Leu        |
|            | <i>COL5A1</i>     | 2   | 189969003 | c.323C>T              | p.Gly108Asp        |
| 2758       | <i>PLEKHG6</i>    | 12  | 6422338   | c.28delG              | p.Glu10Argfs*40    |
| 2859       | <i>HKDC1</i>      | 10  | 70987024  | c.125G>A              | p.Arg42Gln         |
|            | <i>HKDC1</i>      | 10  | 71000508  | IVS6-1G>A             | Splice defect      |
| 3046       | <i>CCDC88B</i>    | 11  | 64118952  | c.2963C>A             | p.Ala988Glu        |
|            | <i>CCDC88B</i>    | 11  | 64119728  | c.3126C>T             | p.Arg1076Trp       |
| 3096       | <i>ARHGAP39</i>   | 8   | 145773344 | c.24_26delTCG         | p.Gln376del        |
| 3168       | <i>LCNL1</i>      | 9   | 139879399 | c.431C>G              | p.Pro144Arg        |
|            | <i>LCNL1</i>      | 9   | 139879435 | c.467T>C              | p.Leu156Pro        |
| 3176       | <i>ECE2</i>       | 3   | 183995077 | c.655C>G              | p.Arg219Gly        |
|            | <i>ECE2</i>       | 3   | 184008893 | c.2253C>T             | p.Arg752Trp        |
| 3242       | <i>SERPINA9</i>   | 14  | 94936088  | c.90C>A               | p.Tyr30*           |
|            | <i>SERPINA9</i>   | 14  | 94929482  | c.1256C>T             | p.Ala419Val        |
| 3412       | <i>TTN</i>        | 2   | 179621363 | c.10327G>T            | p.Glu3443*         |
|            | <i>TTN</i>        | 2   | 179410304 | c.68914G>A            | p.Asp22972Asn      |
| 3415       | <i>TPGS1</i>      | 19  | 507765    | c.259C>T              | p.Pro87Ser         |
|            | <i>TPGS1</i>      | 19  | 519341    | c.7919G>T             | p.Arg264Leu        |
| 3483       | <i>BHLHE22</i>    | 8   | 65493448  | c.101C>G              | p.Ala34Gly         |
|            | <i>BHLHE22</i>    | 8   | 65494020  | c.695_703delGCAGCAGCA | p.Ser232_Ser234del |
| 3495       | <i>CABP1</i>      | 12  | 121093653 | c.43_44delGC          | p.Ala15fs          |
|            | <i>CABP1</i>      | 12  | 121093759 | c.146G>A              | p.Arg49His         |
| 3498       | <i>EYS</i>        | 6   | 65532559  | c.3149C>G             | p.Pro1050Arg       |
|            | <i>EYS</i>        | 6   | 64488046  | c.7751C>G             | p.Thr2584Ser       |
| 3501       | <i>ITIH5</i>      | 10  | 7621958   | c.1178T>C             | p.Ile393Thr        |
|            | <i>ITIH5</i>      | 10  | 7621932   | c.1204G>A             | p.Val402Ile        |

**Table S3: Observed and expected de novo variants in six gene-sets of patients with PH analysed in this study. Related to Figure 1**

| Gene set <sup>‡</sup> | No. of genes | Obs | Nonsense |         | Obs | missense |         |
|-----------------------|--------------|-----|----------|---------|-----|----------|---------|
|                       |              |     | Exp      | P-value |     | Exp      | P-value |
| FMRP                  | 842          | 1   | 0.843    | 0.569   | 7   | 3.579    | 0.099   |
| Chromatin             | 428          | 0   | 0.292    | 1.000   | 1   | 1.236    | 1.000   |
| Embryonic             | 1,912        | 0   | 1.112    | 0.634   | 6   | 4.732    | 0.485   |
| PSD                   | 1,445        | 2   | 0.803    | 0.192   | 5   | 3.414    | 0.403   |
| Essential             | 1,750        | 3   | 1.048    | 0.089   | 4   | 4.457    | 1.000   |
| Mendelian             | 256          | 1   | 0.198    | 0.179   | 1   | 0.841    | 0.569   |

<sup>‡</sup>The six different gene sets analysed in this test, for definitions of names see Supplemental Experimental Procedures. Exact binomial test (two-tailed).



**Table S4: Phenotypic description of patient (i.d 2758) with loss-of-function variant in isoform four of *PLEKHG6*. Related to Figure 1**

| Individual | Clinical description  |
|------------|---|
| 2758       | <p>The individual who was homozygous for the c.26delG variant was the first born male child of unrelated healthy parents. The pregnancy was unremarkable, there was no exposure to known teratogens and his delivery was at term. His birth weight was on the 50<sup>th</sup> centile and head circumference on the 90<sup>th</sup> centile. He was hypotonic in the neonatal period with some episodes of hypoglycemia which responded to treatment satisfactorily. He had bilateral undescended testes and was noted to be dysmorphic. A MRI scan of the head revealed bilateral periventricular nodular heterotopia, predominating in the occipital horns and trigone. There was a megacisterna magna, thinning of the corpus callosum and an ectopic posterior pituitary. He developed localized bronchiectatic changes in his right middle lobe in the first three years of life but a CT chest performed at age 7 demonstrated resolution of these changes. Now aged 7 years he has mild-mod developmental delay but has never had a seizure. Evaluation of his pituitary function has demonstrated no abnormality. His head circumference has tracked the 75<sup>th</sup> centile for age.</p> |

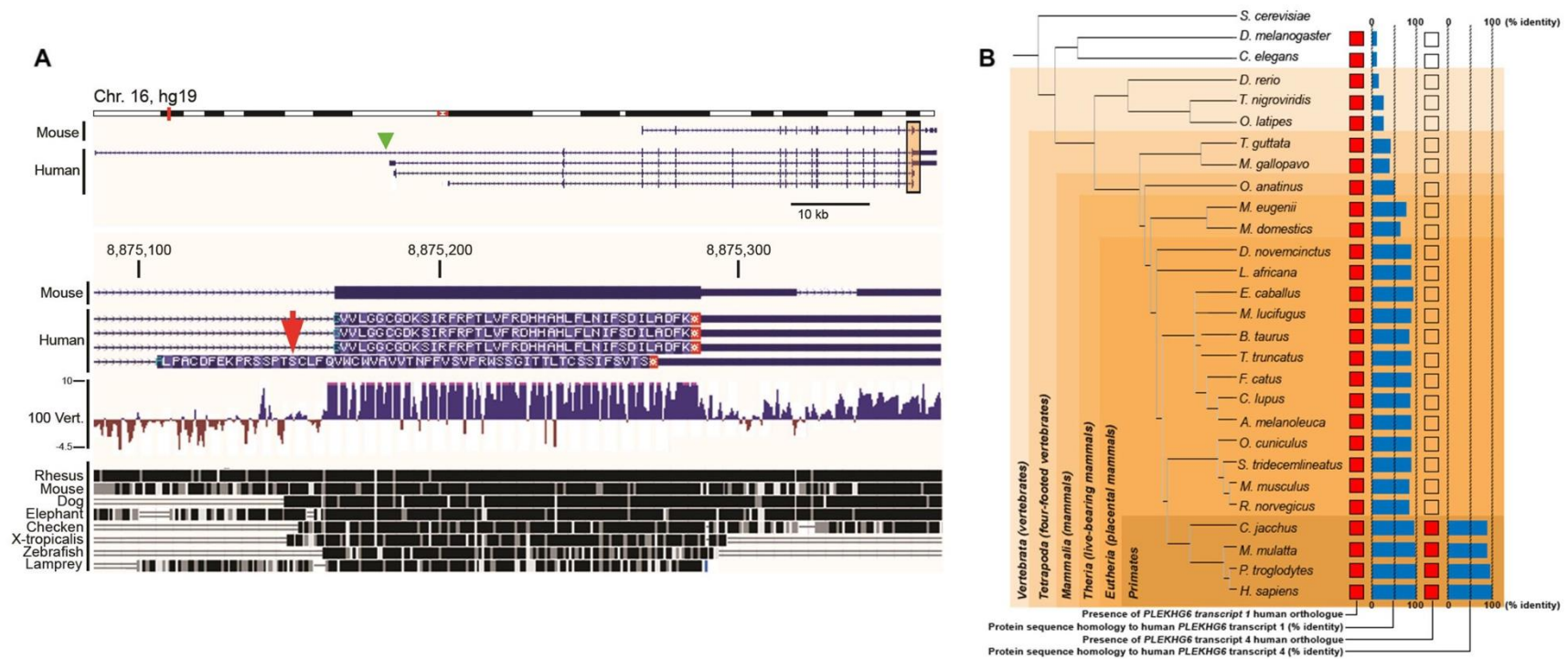


**Figure S1. Additional evolutionarily dynamic isoforms identified through whole-exome sequencing of patients with PH. Related to Figure 1. (A)** UCSC Genome Browser tracks illustrating the *ABAT* loci variant in a patient with PH in an isoform that is not present in mice, but has some experimental support to be present in humans. Top panel outlines the entire locus and the various isoforms annotated experimentally in mice and humans. Orange shade highlights the region shown at higher resolution in the bottom panel. Red arrow identifies the site of the variant in the patient (specific nucleotide residue is outlined in tables S1). 100 Vert. track outlines multiple alignment data for 100 vertebrate species and measurement of evolutionary conservation. Conservation track is also outlined for eight species of varying phylogenetic distances from humans. Areas of black and grey indicate ‘well’ and ‘less’ conserved regions, respectively (as defined by UCSC Genome Browser). Double line represents areas of excessive evolutionary distance between species generating long stretches of reduced homology; same for areas with no double lines or shading. Green arrow head indicates the location of a ‘newly enriched primate specific’ *cis*-regulatory site within the locus, as outlined in (Vermunt et al., 2016). **(B)** Phylogenetic tree outlining the evolutionary relationship among the various species. Red squares indicate orthologue annotations supported by Ensembl, NCBI, and UCSC genome bioinformatics data. Blue shades outline protein sequence homology (% identity) for isoform one and four of humans, first and second column, respectively.

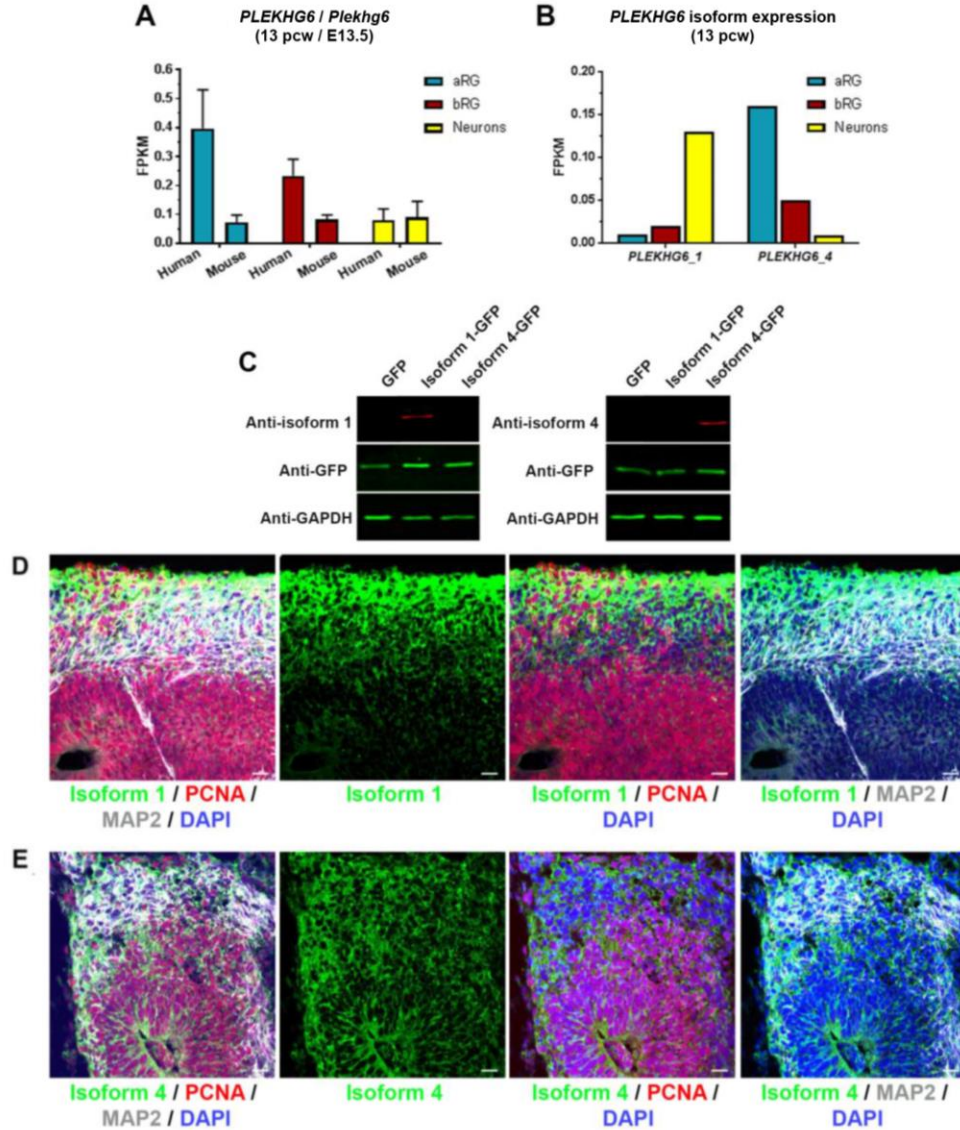


**Figure S2. *PLEKHG6\_1* and *PLEKHG6\_4* are differentially regulated in developing human brain tissue. Related to Figure 1.** (A) Normalised *PLEKHG6* and *Plekhg6* expression levels in 13 post-conceptional week (pcw) human or embryonic day (E) 13.5 mouse apical radial glia (aRG), basal radial glia (bRG), and post-mitotic neurons (N). (B) Normalised expression of *PLEKHG6* isoforms 1 and 4 (*PLEKHG6\_1* and *PLEKHG6\_4*, respectively) of human *PLEKHG6* in the three cell types at 13 pcw. Data in (A) and (B) adapted from (Florio et al., 2015); Error bars, SD. Fragments Per Kilobase of transcript per Million mapped reads (FPKM). n =2 biological replicates. (C) HEK293 cells were transiently transfected with a bi-cistronic vector expressing both green fluorescent protein (GFP) and isoform one or four of *PLEKHG6*. At 24 h after transfection, total cell lysates were prepared and subjected to western blot analysis using anti-isoform one or four antibodies, anti-GFP (transfection control) and anti-GAPDH as a loading control. (D, E) Micrographs of sections of cerebral organoids derived from human iPSCs (day 57 in culture) showing isoform one localisation with MAP2+ cells and isoform four localisation with PCNA+ and MAP2+ cells. Scale bar represents 30  $\mu$ m.

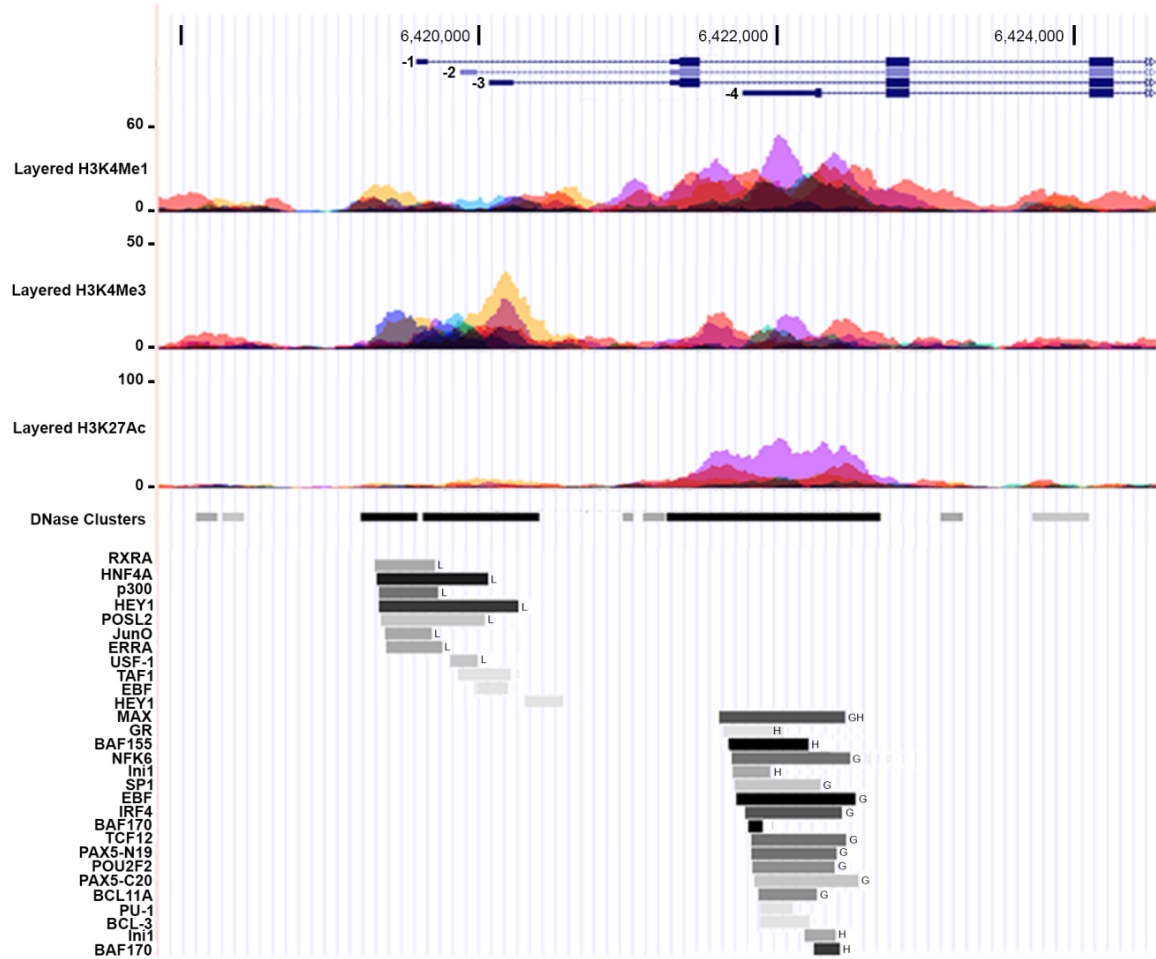


**Figure S3. *PLEKHG6* has alternate isoforms that are potentially differentially regulated in distinct cell types. Related to Figure 1.** Top panel indicates the relative genomic organization of the 5' non-coding first exons of isoforms one to four. Middle panel, reads per million mapped (RPM) normalized ChIP-seq reads for H3K4Me1, H3K4Me3 and H3K27Ac, layered across seven cell lines as outlined by ENCODE (axis limit 100 RPM). Sites of DNase hypersensitivity overlap defined *cis*-regulatory sites. Bottom panel, outlines transcription factor binding analysis at the *PLEKHG6* locus as defined by ChIP-seq data from ENCODE. In total 91 cell lines were assayed for a total of 161 transcription factors. The name of the transcription factors is identified to the left, with the line detected also labeled: L, hepatocellular carcinoma; G, lymphoblastoid; H, HeLa. Note transcription factors overlapping isoform one locus were all identified in hepatocellular carcinoma. In contrast, transcription factors overlapping isoform four were detected in either lymphoblastoid or HeLa cells.



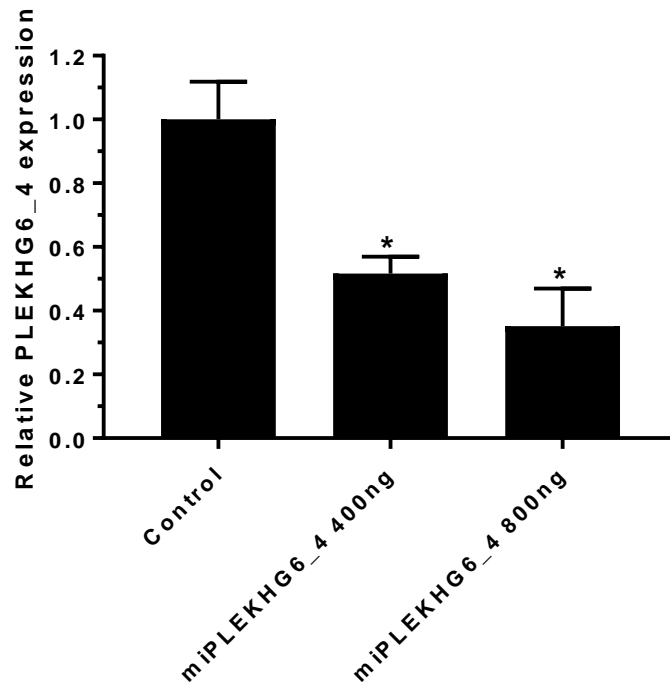


**Figure S4. Validation of the miRNA targeting the primate specific isoform of PLEKHG6 (PLEKHG6\_4). Related to Figure 2.** Efficiency of miRNA knockdown targeted by PLEKHG6\_4 (miPLEKHG\_4) at 400ng and 800ng was determined by transient co-transfection with a PLEKHG6\_4 expression plasmid (pcDNA3.1V5/His-PLEKHG6\_4), and data expressed as relative PLEKHG6\_4 expression. Relative expression of PLEKHG6\_4 was calculated for each miPLEKHG\_4 sample as the ratio of PLEKHG6\_4 expression to mock transfected control via Western blot, using anti-V5 antibody to detect PLEKHG6 expression. Data presented as mean ( $\pm$  S.E.M). Mann-Whitney U test; \*  $p < 0.05$ .  $n = 3$ .

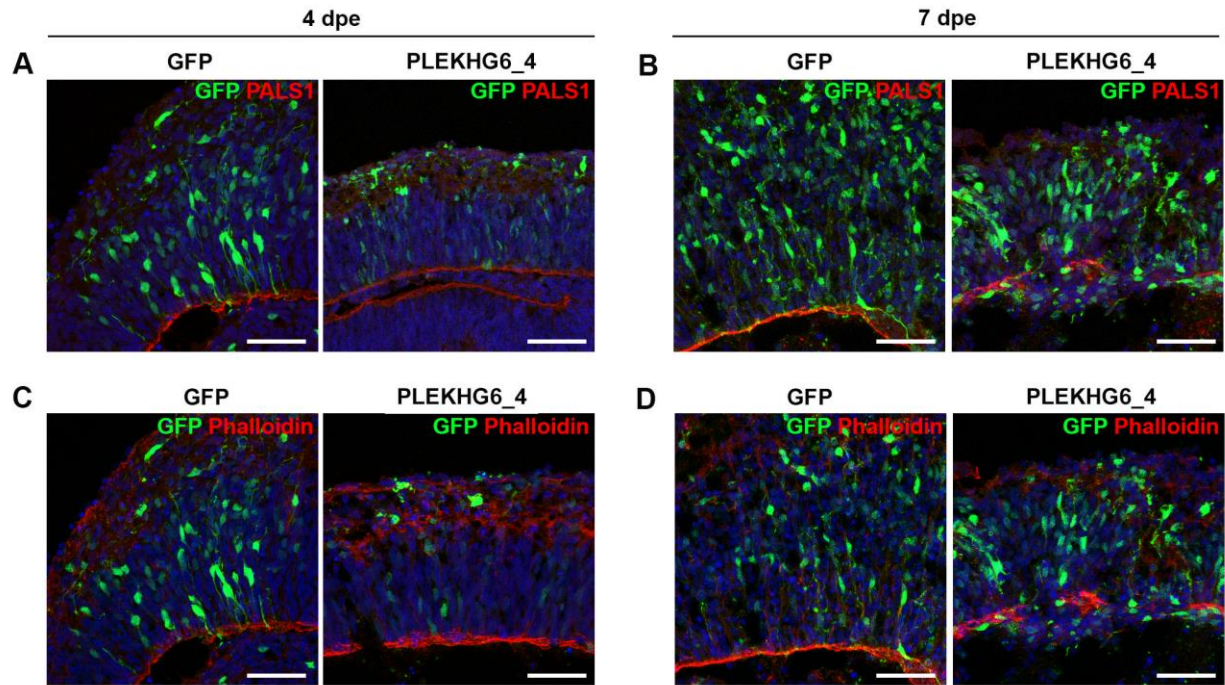


**Figure S5. Progressive disruption of ventricular integrity in organoids overexpressing *PLEKHG6\_4*. Related to Figure 3.** (A, D) Micrographs sections of day 42 human cerebral organoids electroporated with GFP/empty vector control or human *PLEKHG6* isoform 4 (*PLEKHG6\_4*) and analysed four (A, C) or seven (B, D) days post electroporation, 4 dpe and 7 dpe, respectively. Sections were then immunostained for PALS1 or Phalloidin as indicated. Scale bar represents 30 μm.

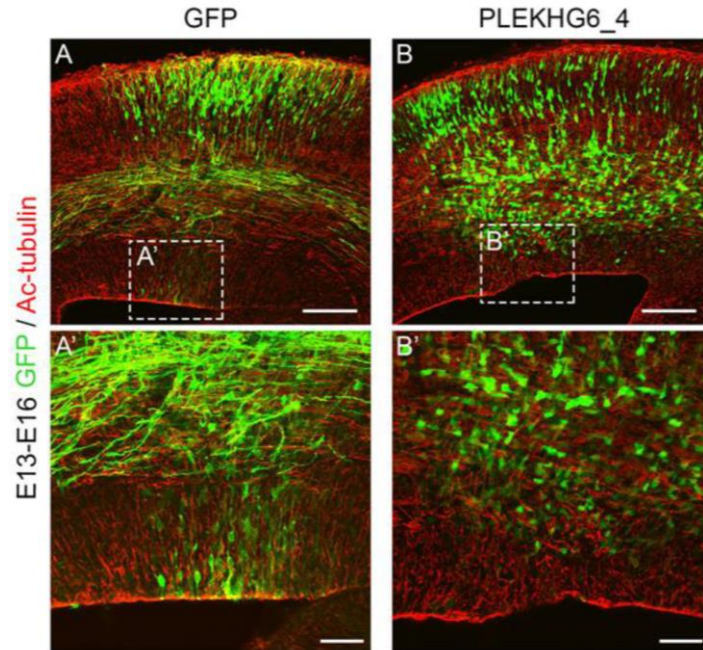


**Figure S6. PLEKHG6\_4 expression in the developing mouse cortex disrupts radial glia processes. Related to Figure 4.** Coronal micrograph sections of E16 mouse cerebral cortices electroporated at E13 with (A) GFP/empty vector control or (B) human PLEKHG6 isoform 4 (PLEKHG6\_4) and stained for GFP and acetylated tubulin (Ac-tubulin). (A', B') Higher magnifications of (A) and (B) showing disrupted radial glia processes upon PLEKHG6\_4 overexpression. Scale bar represents (A, B) 100  $\mu$ m and (A', B') 50  $\mu$ m.

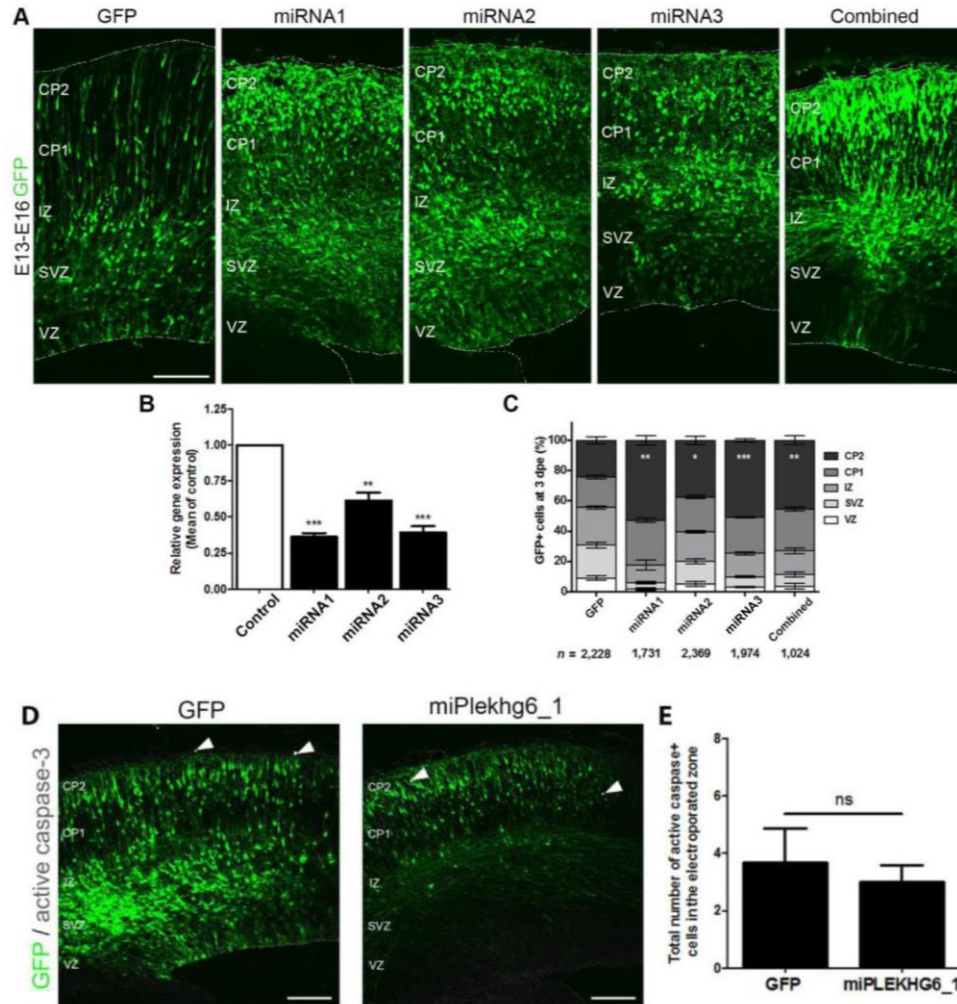


**Figure S7. microRNA (miRNA) validation studies. Related to Figure 5.** (A) Coronal micrograph sections of E16 mouse cerebral cortices electroporated at E13 with GFP/empty vector control, *Plekhg6* microRNAs (miRNA1,2,3 or combined). (B) Mean ( $\pm$  s.e.m) *Plekhg6* expression in P19 cells (n=3) 24 hours post transfection (1.5  $\mu$ g) with one of three miRNA targeting *Plekhg6* relative to control treated sample (empty vector) expression using the delta-delta Ct method, as determined by real-time PCR. Expression was normalised against *GAPDH* and *DIMT1* housekeeping genes in the same sample using the relative standard curve method. (C) Quantification of the distribution of GFP-expressing (GFP+) cells transfected with GFP/empty vector alone or *Plekhg6* miRNAs (miRNA1, 2 and 3) 3 days after electroporation (mean  $\pm$  s.e.m). (D) Coronal micrograph sections of E16 mouse cerebral cortices electroporated at E13 with GFP/empty vector control or *Plekhg6* targeting miRNAs (miPlekhg6). White arrows outline cells staining for active-caspase within the electroporated zone. Quantification of the total number of active caspase cells in the electroporated region within the treatment groups are presented as mean  $\pm$  s.e.m (E). At least three embryos analysed for each condition. n, total number of GFP+ cells counted per condition. Mann-Whitney U test; \*  $p < 0.05$ ; \*\*  $p < 0.01$ ; \*\*\*  $p < 0.001$ . Scale bar represents 100  $\mu$ m.